AFRL-VA-WP-TP-2006-323

EFFICIENT RECONFIGURATION AND RECOVERY FROM DAMAGE FOR AIR VEHICLES (PREPRINT)

Michael W. Oppenheimer and David B. Doman

JULY 2006

Approved for public release; distribution is unlimited.

STINFO COPY

AIR VEHICLES DIRECTORATE
AIR FORCE MATERIEL COMMAND
AIR FORCE RESEARCH LABORATORY
WRIGHT-PATTERSON AIR FORCE BASE, OH 45433-7542

NOTICE AND SIGNATURE PAGE

AFRL-VA-WP-TP-2006-323 HAS BEEN REVIEWED AND IS APPROVED FOR PUBLICATION IN ACCORDANCE WITH ASSIGNED DISTRIBUTION STATEMENT.

*//Signature//

David B. Doman
Senior Aerospace Engineer
Control Design and Analysis Branch
Air Force Research Laboratory
Air Vehicles Directorate

//Signature//

Deborah S. Grismer
Chief
Control Design and Analysis Branch
Air Force Research Laboratory
Air Vehicles Directorate

//Signature//

JEFFREY C. TROMP
Senior Technical Advisor
Control Sciences Division
Air Vehicles Directorate

This report is published in the interest of scientific and technical information exchange, and its publication does not constitute the Government's approval or disapproval of its ideas or findings.

*Disseminated copies will show "//Signature//" stamped or typed above the signature blocks.

REPORT DOCUMENTATION PAGE

Form Approved
OMB No. 0704-0188

1. REPORT DATE *(DD-MM-YY)*	2. REPORT TYPE	3. DATES COVERED *(From - To)*
July 2006	Conference Paper Preprint	01/01/2006 – 06/30/2006

4. TITLE AND SUBTITLE
EFFICIENT RECONFIGURATION AND RECOVERY FROM DAMAGE FOR AIR VEHICLES (PREPRINT)

5a. CONTRACT NUMBER
In-house

5b. GRANT NUMBER

5c. PROGRAM ELEMENT NUMBER
62201F

6. AUTHOR(S)
Michael W. Oppenheimer and David B. Doman

5d. PROJECT NUMBER
A03D

5e. TASK NUMBER

5f. WORK UNIT NUMBER
0B

7. PERFORMING ORGANIZATION NAME(S) AND ADDRESS(ES)
Control Design and Analysis Branch (AFRL/VACA)
Control Sciences Division
Air Vehicles Directorate
Air Force Materiel Command, Air Force Research Laboratory
Wright-Patterson Air Force Base, OH 45433-7542

8. PERFORMING ORGANIZATION REPORT NUMBER
AFRL-VA-WP-TP-2006-323

9. SPONSORING/MONITORING AGENCY NAME(S) AND ADDRESS(ES)
Air Vehicles Directorate
Air Force Research Laboratory
Air Force Materiel Command
Wright-Patterson Air Force Base, OH 45433-7542

10. SPONSORING/MONITORING AGENCY ACRONYM(S)
AFRL-VA-WP

11. SPONSORING/MONITORING AGENCY REPORT NUMBER(S)
AFRL-VA-WP-TP-2006-323

12. DISTRIBUTION/AVAILABILITY STATEMENT
Approved for public release; distribution is unlimited.

13. SUPPLEMENTARY NOTES
Report contains color.

This work has been submitted to the 2006 AIAA Guidance, Navigation, and Control Conference proceedings. This is a work of the U.S. Government and is not subject to copyright protection in the United States.

PAO Case Number: AFRL/WS 06-1816 (cleared July 26, 2006).

14. ABSTRACT

The integration of health management, fault detection and isolation with trajectory reshaping and adaptive guidance and control is a natural and necessary step in producing reliable and responsive autonomous aerospace vehicles. The benefits of reconfigurable control and trajectory reshaping have been demonstrated; however, in many cases these results relied upon the assumption that IVHM/FDI systems provided specific information to the algorithms. Requirements on IVHM/FDI from the perspective of guidance, control and trajectory reshaping have been listed and some opportunities for synergistic information exchange between the two systems have been identified.

15. SUBJECT TERMS
Integrated Vehicle Health Management, Fault Detection and Isolation, Adaptive Guidance, Reconfigurable Control

16. SECURITY CLASSIFICATION OF:			17. LIMITATION OF ABSTRACT:	18. NUMBER OF PAGES	19a. NAME OF RESPONSIBLE PERSON (Monitor)
a. REPORT	b. ABSTRACT	c. THIS PAGE			David B. Doman
Unclassified	Unclassified	Unclassified	SAR	36	19b. TELEPHONE NUMBER *(Include Area Code)* N/A

Standard Form 298 (Rev. 8-98)
Prescribed by ANSI Std. Z39-18

Efficient Reconfiguration and Recovery From Damage for Air Vehicles *

Michael W. Oppenheimer †
David B. Doman ‡
Air Force Research Laboratory, WPAFB, OH 45433-7531

In order to increase survivability and maximize performance, autonomous vehicles will require the development of algorithms that fulfill the role of an adaptive human pilot in response to failures, damage, or uncertain vehicle dynamics. Hence, the guidance and control algorithms implemented on autonomous vehicles must be able to react and compensate, whenever possible, for failures so that the impact of a failure can be minimized. A great deal of progress has been made over the past decade in the development of trajectory reshaping algorithims, adaptive guidance and reconfigurable control; however, much of this work is dependent upon future developments in integrated vehicle health management (IVHM). This manuscript will highlight how four recent guidance, control and trajectory reshaping methods methods rely on fault detection and isolation (FDI) and IVHM capabilities to respond to failures or damage to the vehicle. The first is an adaptive reconfigurable inner-loop controller for a space maneuvering vehicle. The purpose of this inner-loop control system is to accurately track body-frame angular velocity vector commands, while automatically reacting to and compensating for control effector failures. The control reconfiguration is performed by the control allocator, which, in this case, is a linear programming based algorithm, suitable for implementation on today's flight computers. Control allocators of this type enforce rate and position limits on the actuators which may change depending on the nature of the failure. IVHM will be required to provide control failure information to the control allocator which may include changes to these limits or changes to the actuator dynamics. The allocator does not take into account actuator dynamics; however, a post processing method can be used to compensate for the interactions between constrained control allocators and actuator dynamics. One advantage of this method is that there is little additional computational overhead, thus allowing implementation on today's aircraft. The third method uses online system identification to compensate for modeling error or damage to an aerodynamic control surface and could be used to augment IVHM or FDI to identify changes to the control effectiveness matrix, which can in-turn be used to update the control allocator. The last problem addressed in this work is recovery from damage to a vehicle which results in a change to the outer mold line. Trajectory reshaping, in particular, requires information about how an damage or failure induced conditions affect the vehicle at future flight conditions. For a locked control effector, the effects can be quantified in the nominal aerodynamic database, even at future flight conditions. However, when damage occurs to a vehicle, the nominal aerodynamic database is most likely no longer accurate. Use of the nominal database to estimate failure effects at future flight conditions can have dire consequences since the aircraft lift, drag and moment generating capabilities can change resulting in high or low energy conditions at key locations in the trajectory. Hence, it is important to have the capacity to generate accurate estimates of the effects of damage. Here, a method is discussed which has the potential to allow recovery from damage, when it is physically possible to do so. The underlying idea is to utilize a fast and efficient algorithm to estimate the new aerodynamic database, after damage has occurred. Algorithms for generating a new aerodynamic database is used in the control laws to provide a more accurate representation of the vehicle. The required inputs to this

†Electronics Engineer, 2210 Eighth Street, Bldg. 146, Rm. 305, Ph. 937-255-8490, Email Michael.Oppenheimer@wpafb.af.mil

‡Senior Aerospace Engineer, 2210 Eighth Street, Bldg. 146, Rm. 305, Ph. 937-255-8451, Email David.Doman@wpafb.af.mil

algorithm would be provided by an advanced IVHM system and would require advances in the state of the art. These requirements are outlined here to communicate the needs of the GN&C community to the IVHM/FDI community.

I. Introduction

In this work, four methods are discussed for identification and/or recovery from failures/damage. The first technique described, accounts for control effector failures, which utilizes three layers of reconfiguration. The starting point is a reconfigurable inner-loop control law, where control effectors are re-mixed to account for a locked or floating effector. The control effector failure information is supplied by a health monitoring system. The reconfigurable inner-loop control law is based on dynamic inversion with explicit model following coupled with an optimization based control allocator. The dynamic inversion control law[1] requires the use of a control effector allocation algorithm, if the number of control effectors exceeds the number of controlled variables or if actuator rate and position limits must be enforced. Illustrative examples of the methods will be used throughout the paper and will make use of a vehicle that has 6 control surfaces, namely, left and right ruddervators, left and right flaperons, speedbrake, and bodyflap. Because there are 6 control surfaces and only 3 axes to control, it is possible that the desired control variable rate commands can be achieved in many different ways and so a control allocation algorithm is used to provide a unique solution to such problems.[2,3] To complete the inner-loop, prefilter blocks are designed to produce the desired closed-loop dynamics. In this work, an explicit model-following prefilter scheme is introduced so the inner-loop bandwidth can be adjusted by modifying the bandwidth of the explicit model when all control power is exhausted in one or more axes. The second layer of reconfiguration, namely, guidance adaptation, becomes active when this situation occurs (called axis saturation or control power deficiency). When a control power deficiency is detected, the bandwidth of the reference model in the explicit model following system is reduced in order to decrease the magnitude of the angular acceleration commands being passed to the control allocator. Since the angular accelerations are taken to be monotonic functions of control surface deflections, reducing the magnitude of the angular acceleration command decreases the magnitude of the surface deflections, thereby driving them away from saturation. When the closed inner-loop bandwidth is reduced in this way, the gains in the outer-loop guidance system must also be modified to preserve acceptable stability margins, hence, this information (bandwidth) is passed to the adaptive guidance loop.[4] The third layer of reconfiguration is trajectory reshaping. Under certain control failure scenarios, the perturbations to trim lift and drag can be significant enough that following the nominal trajectory will result in large (possibly catastrophic) errors in the terminal condition. These perturbations are typically the combined result of unfailed control effectors being forced to off-nominal positions to counter the effect of failed effectors in an attempt to maintain rotational equilibrium. In such cases inner-loop reconfiguration and guidance adaptation are not sufficient to recover the vehicle and the trajectory can in some cases be modified such that desired terminal conditions can be recovered.

One item that is not considered in the reconfigurable control law is the effect of actuator dynamics. In fact, nearly all control allocation methods assume that the actuator dynamics have infinite bandwidth, that is, a control command is exactly and instantly supplied by the control effectors. While this assumption simplifies the control mixing problem, there are cases where the actuator dynamics must be taken into account. For such cases, a method is presented which post-processes the outputs of a control allocator, to account for actuator dynamics.

The third failure identification method involves system identification, in particular, estimation of the control effectiveness matrix when effectors are damaged or failed. The method described can be used to augment an IVHM system.

The fourth method for failure recovery deals with damage to vehicles. One of the main difficulties in trajectory reshaping is predicting the effects of failures or damage at future flight conditions. A method is presented that can generate critical information that is required to perform on-line trajectory reshaping. In particular, a method for estimating failure induced constraints, for failures involving locked or floating control effectors, is presented which accounts for 6 degree-of-freedom (DOF) effects upon the reduced order models that are used by trajectory generation algorithms. These constraints on the vehicle are not constant and can vary widely over different flight conditions. This means that one cannot assume that a set of constraints estimated at a one flight condition will be valid at any other flight condition. This phenomenon limits the class of failures for which one can estimate constraints or 6 DOF effects on reduced order models, using only

the original aerodynamic database. Effector failures such as locked or floating surfaces are a class of failures whose effects can be estimated over a wide range of operating conditions. This is because the aerodynamic database for the vehicle does not change as a result of such a failure. The effects of locked or floating surfaces can be estimated at all flight conditions for which the original aerodynamic database is valid.

This paper is orgainzed as follows: Section II discusses the inner-loop reconfigurable controller and Section III presents the scheme for accounting for actuator dynamics in a reconfigurable control law. Section IV discussed the identification of control effectiveness, Section V looks at the issues involved with vehicle recovery from damage, while conclusions are presented in Section VII.

II. Reconfigurable Inner-Loop Controller

Dynamic inversion control laws are well suited for use as a baseline system for reconfigurable control. This is because the control law can easily be written in terms of the vehicle equations of motion and of the aerodynamic coefficients. If any of the model parameters change as a result of failure or damage, estimates of the new parameters from IVHM or on-line system identification can be used to update the control law on-line.

To illustrate the how such a system operates, we consider a space maneuvering vehicle with 6 control surfaces,[5] namely, left and right flaperons, left and right ruddervators, a speedbrake and a bodyflap. An outer-loop adaptive guidance system generates body-frame angular velocity commands (p_{des}, q_{des}, r_{des}), that the inner-loop control system attempts to track. The dynamics of the body-frame angular velocity vector for a lifting body can be written as

$$\dot{\boldsymbol{\omega}} = \mathbf{f}(\boldsymbol{\omega}, \mathbf{P}) + \mathbf{g}(\mathbf{P}, \boldsymbol{\delta}) \tag{1}$$

where $\boldsymbol{\omega} = [\text{p q r}]^T$, p, q, and r are the rolling, pitching, and yawing rates, respectively, $\mathbf{P}$ denotes measurable or estimable quantities that influence the body-frame states, and $\boldsymbol{\delta} = (\delta_1, \delta_2, \cdots, \delta_n)^T$ is a vector of control surface deflections. The vector $\mathbf{P}$ contains variables such as angle of attack, sideslip, Mach number, and vehicle mass properties. The term $\mathbf{g}(\mathbf{P}, \boldsymbol{\delta})$ includes the control dependent accelerations, while the term $\mathbf{f}(\boldsymbol{\omega}, \mathbf{P})$ describes accelerations that are due to the base-vehicle's (wing-body) aerodynamic properties. Here it is assumed that the mass properties of the vehicle are constant, although the variable mass case could easily be handled if mass property estimates were available through an IVHM system. Under the assumption of constant mass, the time derivative of the inertia matrix can be set to zero, i.e., $\dot{\mathbf{I}} = \mathbf{0}$. Then, Equation 1 can be written as[6]

$$\dot{\boldsymbol{\omega}} = \mathbf{I}^{-1}(\mathbf{G}_B(\boldsymbol{\omega}, \mathbf{P}, \boldsymbol{\delta}) - \boldsymbol{\omega} \times \mathbf{I}\boldsymbol{\omega}) \tag{2}$$

where

$$\mathbf{G}_B(\boldsymbol{\omega}, \mathbf{P}, \boldsymbol{\delta}) = \mathbf{G}_{WB}(\boldsymbol{\omega}, \mathbf{P}) + \mathbf{G}_\delta(\mathbf{P}, \boldsymbol{\delta}) = \begin{bmatrix} L \\ M \\ N \end{bmatrix}^T_{WB} + \begin{bmatrix} L \\ M \\ N \end{bmatrix}^T_{\delta} \tag{3}$$

In Equations 2 and 3, $\mathbf{I}$ is the inertia matrix and L, M, and N are the rolling, pitching, and yawing moments. In Equation 3, $\mathbf{G}_{WB}(\boldsymbol{\omega}, \mathbf{P})$ is the moment generated by the base aerodynamic system (wing-body system) and $\mathbf{G}_\delta(\mathbf{P}, \boldsymbol{\delta})$ is the total moment vector produced by the control effectors. Therefore,

$$\begin{aligned} \mathbf{f}(\boldsymbol{\omega}, \mathbf{P}) &= \mathbf{I}^{-1}[\mathbf{G}_{WB}(\boldsymbol{\omega}, \mathbf{P}) - \boldsymbol{\omega} \times \mathbf{I}\boldsymbol{\omega}] \\ \mathbf{g}(\mathbf{P}, \boldsymbol{\delta}) &= \mathbf{I}^{-1}\mathbf{G}_\delta(\mathbf{P}, \boldsymbol{\delta}) \end{aligned} \tag{4}$$

In order to utilize a linear control allocator, it is necessary that the control dependent portion of the model be linear in the controls. Hence, an affine approximation is developed such that

$$\mathbf{G}_\delta(\mathbf{P}, \boldsymbol{\delta}) \approx \widetilde{\mathbf{G}}_\delta(\mathbf{P})\boldsymbol{\delta} + \boldsymbol{\epsilon}(\mathbf{P}, \boldsymbol{\delta}) \tag{5}$$

The term $\boldsymbol{\epsilon}(\mathbf{P}, \boldsymbol{\delta})$ is an intercept term[7] for the body-axis angular accelerations which is used to improve the accuracy of linear control allocation algorithms. Using Equations 1, 4, and 5, the model used for the design of the dynamic inversion control law becomes

$$\dot{\boldsymbol{\omega}} = \mathbf{f}(\boldsymbol{\omega}, \mathbf{P}) + \mathbf{I}^{-1}\widetilde{\mathbf{G}}_\delta(\mathbf{P})\boldsymbol{\delta} + \mathbf{I}^{-1}\boldsymbol{\epsilon}(\mathbf{P}, \boldsymbol{\delta}) \tag{6}$$

The objective is to find a control law, that provides direct control over $\dot{\boldsymbol{\omega}}$, so that $\dot{\boldsymbol{\omega}} = \dot{\boldsymbol{\omega}}_{des}$. Hence, the inverse control law must satisfy

$$\dot{\boldsymbol{\omega}}_{des} - \mathbf{f}(\boldsymbol{\omega}, \mathbf{P}) - \mathbf{I}^{-1}\boldsymbol{\epsilon}(\mathbf{P}, \boldsymbol{\delta}) = \mathbf{I}^{-1}\widetilde{\mathbf{G}}_{\delta}(\mathbf{P})\boldsymbol{\delta} \tag{7}$$

Equation 7 provides the dynamic inversion control law that is used to set up a control allocation problem.

A. CONTROL ALLOCATION

Since there are more control effectors (6) than controlled variables (3) and the control effectors are restricted by position and rate limits, a control allocation algorithm is necessary. For inner-loop control, there are three controlled variables, namely, roll, pitch, and yaw accelerations, while there are six control surfaces. Hence, a control allocation scheme must be used to insure that Equation 7 is satisfied. The control allocation scheme uses the mixed optimization linear programming technique of Bodson.[3]

To begin development of the allocator, let the left-hand side of Equation 7 be defined as $\mathbf{d}_{des}$ and denote the right-hand side of Equation 7 as $\mathbf{B}\boldsymbol{\delta}$. Here, $\mathbf{d}_{des}$ are the body-axis accelerations that must be produced by the control effectors and $\mathbf{B}$ is the control effectiveness matrix defined as

$$\mathbf{B} = \mathbf{I}^{-1}\widetilde{\mathbf{G}}_{\delta}(\mathbf{P}) = \mathbf{I}^{-1}\begin{bmatrix} \frac{\partial L}{\partial \delta_1} \frac{\partial L}{\partial \delta_2} \cdots \frac{\partial L}{\partial \delta_n} \\ \frac{\partial M}{\partial \delta_1} \frac{\partial M}{\partial \delta_2} \cdots \frac{\partial M}{\partial \delta_n} \\ \frac{\partial N}{\partial \delta_1} \frac{\partial N}{\partial \delta_2} \cdots \frac{\partial N}{\partial \delta_n} \end{bmatrix} \tag{8}$$

The following mixed optimization problem can be posed, which solves the error minimization problem and, if sufficient control authority exists, minimizes the difference between the control effector positions and a preferred set of effector positions (control minimization problem):

$$\min_{\delta} \left(\|\mathbf{B}\boldsymbol{\delta} - \mathbf{d}_{des}\|_1 + \lambda \|\mathbf{W}_{\delta}(\boldsymbol{\delta} - \boldsymbol{\delta}_p)\|_1 \right) \tag{9}$$

subject to

$$\overline{\boldsymbol{\delta}} \leq \boldsymbol{\delta} \leq \underline{\boldsymbol{\delta}} \tag{10}$$

where $\underline{\boldsymbol{\delta}}$, $\overline{\boldsymbol{\delta}}$ are the most restrictive lower and upper limits on the control effectors, respectively, and the 1-norm is selected so that linear programming techniques can be used to solve the problem.[3] In Equation 9, the parameter λ is used to weight the error and control minimization problems. For this work, it was determined that $\lambda = 0.01$ provided good error minimization while still driving the control effectors to the preferred values when sufficient control authority existed. The most restrictive lower and upper limits on the control effectors are specified as

$$\begin{aligned} \overline{\boldsymbol{\delta}} &= \min(\boldsymbol{\delta}_U, \boldsymbol{\delta} + \dot{\boldsymbol{\delta}}_{max}\Delta t) \\ \underline{\boldsymbol{\delta}} &= \max(\boldsymbol{\delta}_L, \boldsymbol{\delta} - \dot{\boldsymbol{\delta}}_{max}\Delta t) \end{aligned} \tag{11}$$

where $\boldsymbol{\delta}_L, \boldsymbol{\delta}_U$ are the lower and upper position limits, $\boldsymbol{\delta}$ is the last control effector command from the control allocation algorithm, $\dot{\boldsymbol{\delta}}_{max}$ is a vector of rate limits, and Δt is the timestep or control update rate.

The vector $\boldsymbol{\delta}_p$ in Equation 9 is a preference vector. When sufficient control authority exists to drive the norm of acceleration errors to a sufficiently small value, the allocation algorithm will attempt to minimize the difference between the actual control deflections and $\boldsymbol{\delta}_p$. The preference vector is taken to be the pseudo-inverse solution so that

$$\boldsymbol{\delta}_p = -\mathbf{c} + \mathbf{W}^{-1}\mathbf{B}^T(\mathbf{B}\mathbf{W}^{-1}\mathbf{B}^T)^{-1}[\mathbf{d}_{des} + \mathbf{B}\mathbf{c}] \tag{12}$$

where $\mathbf{c}$ is an offset vector and $\mathbf{W}$ is a diagonal weighting matrix of the form

$$\mathbf{W} = \text{diag}[W_{\delta_{RF}}\ W_{\delta_{LF}}\ W_{\delta_{RR}}\ W_{\delta_{LR}}\ W_{\delta_{SB}}\ W_{\delta_{BF}}] \tag{13}$$

The elements of the offset vector $\mathbf{c}$ are all zero except for the elements corresponding to locked control surfaces. If a control effector is locked, then the corresponding entry in $\mathbf{c}$ is set to the negative of the locked location. Also, $\mathbf{W}_{\delta}$ in Equation 9 is a matrix used to weight the importance of driving each control effector to its preferred value. Using this preference vector allows one to analytically represent the control allocator in a robustness analysis of this system that is valid as long as no single axis is saturated and the commanded accelerations are feasible.

B. EXPLICIT MODEL FOLLOWING

The inner-loop flight control system described in the previous section was designed so that the closed-inner-loop system would exhibit a decoupled first order response to body-axis angular rate commands. An explicit model following scheme can be used to shape the closed-inner-loop response and to compensate for modelling errors in the dynamic inversion control law. The for a first order response, desired roll, pitch, and yaw dynamics are described by:

$$\frac{\omega_m(s)}{\omega_{cmd}(s)} = \frac{K_{bw}}{s + K_{bw}} \tag{14}$$

where ω_m denotes either the desired roll, pitch, or yaw rate response of the explicit model and ω_{cmd} denotes the angular velocity command from the guidance and control interface. The term K_{bw} defines the nominal bandwidth of the desired dynamics. The system is designed to provide perfect tracking of the reference model when the dynamic inversion is perfect. Since this is never the case in practice, error compensation elements are used to mitigate the effects of inversion error. If the inversion is perfect, then the controlled element from the point of view of the explicit model following structure is a simple integrator. From block diagram algebra (see Figure 1), one can see that if the controlled element is a simple integrator, that is, if $\omega(s) = \frac{1}{s}\dot{\omega}_{des}(s)$, the $\omega(s)/\omega_m(s)$ transfer function is given by:

$$\frac{\omega(s)}{\omega_m(s)} = \frac{(K_D + K_{FF})s^2 + K_P s + K_I}{(K_D + 1)\, s^2 + K_P s + K_I} \tag{15}$$

which, when $K_{FF} = 1$, results in a double stable pole-zero cancellation with appropriate choices of K_P, K_I, and K_D. Then, it is easily seen that

$$\frac{\omega(s)}{\omega_{cmd}(s)} = \frac{K_{bw}}{s + K_{bw}} \tag{16}$$

and perfect model following is achieved.

C. INTEGRATOR ANTI-WINDUP AND REFERENCE MODEL BANDWIDTH ATTENUATION

When all control power has been exhausted in one or more axes, axis saturation has occurred. Control effector saturation results when one or more control surfaces is moving at its rate limit or lies on a position limit. In this case, control effector saturation is a necessary, but not sufficient, condition for the occurrence of axis saturation. Axis saturation can be detected through an analysis of the control allocation inputs and outputs. If $\mathbf{B}\boldsymbol{\delta} - \mathbf{d}_{des} \neq \mathbf{0}$ then axis saturation has occurred. When an axis is saturated, all control authority has been expended and tracking errors can grow large. In order to prevent the integrator in the explicit model following prefilter from attempting to cancel tracking errors caused by axis saturation, an integrator anti-windup law is used to reduce the magnitude of the input to the integrator. The integrator anti-windup vector used in this design is given by:

$$\mathbf{I}_{aw} = \mathbf{K}_{AW}(\mathbf{B}\boldsymbol{\delta} - \mathbf{d}_{des}) \tag{17}$$

where $\mathbf{K}_{AW}$ is a gain. The integrator antiwindup compensation scheme operates on the difference between the output of the control allocator's internal model of the acceleration-deflection relationship, $\mathbf{B}\boldsymbol{\delta}$, and the desired control effector induced accelerations, $\mathbf{d}_{des}$. If no axes are saturated, then $\mathbf{B}\boldsymbol{\delta} - \mathbf{d}_{des} = \mathbf{0}$ and the control system operates normally. When $\mathbf{B}\boldsymbol{\delta} - \mathbf{d}_{des} \neq \mathbf{0}$, at least one axis is saturated and the state of the prefilter integrator is reduced by the anti-windup signal.

When an axis saturates, that is, when at least one component of $\mathbf{B}\boldsymbol{\delta} - \mathbf{d}_{des} \neq \mathbf{0}$, the inner-loop control system becomes degraded and most likely will not be able to track the nominal commands. One way of conveying this information to an outer-loop guidance command system is by way of inner-loop bandwidth. Nominally, the inner-loop bandwidth is set to K_{bw}, however, when axis saturation occurs, this bandwidth is reduced to avoid overdriving the actuators. The law used to reduce the inner-loop bandwidth is as follows: for all three axes, the input to the reduction law is $|\mathbf{B}\boldsymbol{\delta} - \mathbf{d}_{des}|$ and this is passed through a saturation block which, for the roll channel, is defined as

$$P_{sat} = \begin{cases} 0 \;\; if \;\; |\mathbf{B}\boldsymbol{\delta} - \mathbf{d}_{des}|_P < 0 \\ |\mathbf{B}\boldsymbol{\delta} - \mathbf{d}_{des}|_P \;\; if \;\; 0 \leq |\mathbf{B}\boldsymbol{\delta} - \mathbf{d}_{des}|_P \leq 1 \\ 1 \;\; if \;\; |\mathbf{B}\boldsymbol{\delta} - \mathbf{d}_{des}|_P > 1 \end{cases} \tag{18}$$

Similar definitions are also made for the pitch and yaw channels. Now, the modified or new bandwidths $(K_{bw_P}, K_{bw_Q}, K_{bw_R})$ are defined by

$$\begin{aligned} K_{bw_P} &= \left(\tfrac{-9}{10} P_{sat} + 1\right) K_{bw_{P\,nom}} \\ K_{bw_Q} &= \left(\tfrac{-5}{6} Q_{sat} + 1\right) K_{bw_{Q\,nom}} \\ K_{bw_R} &= \left(\tfrac{-9}{10} R_{sat} + 1\right) K_{bw_{R\,nom}} \end{aligned} \tag{19}$$

where $K_{bw_{P\,nom}}, K_{bw_{Q\,nom}}, K_{bw_{R\,nom}}$ are the nominal bandwidths.

Figure 1 shows the complete inner-loop block diagram while Figure 2 reveals the bandwidth modification logic. Displayed in Figure 1 are the prefilters, dynamic inversion, control allocation, and the integrator antiwindup scheme. For implementation in a digital simulation, all continuous time blocks were converted to equivalent discrete time blocks using a Tustin transformation.

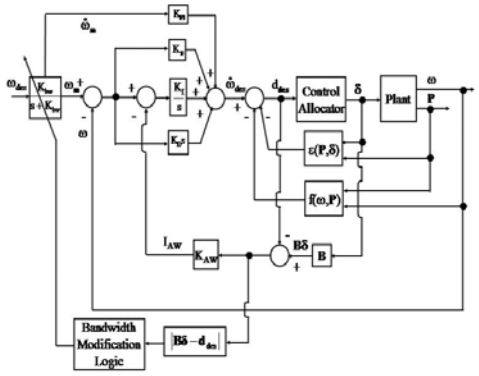

Figure 1. Inner-Loop Block Diagram.

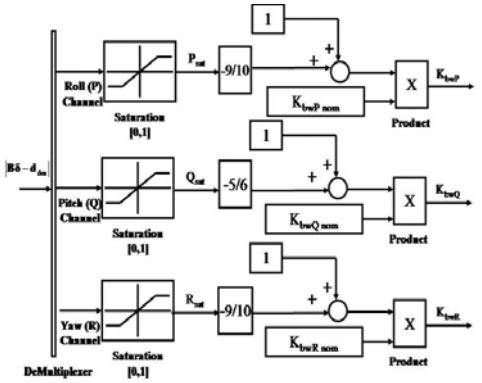

Figure 2. Bandwidth Modification Logic.

D. Implications for IVHM/FDI

The reconfigurable control law described above relies on information from an IVHM/FDI system. In particular, actuator health must be monitored in such a way that locked control effectors can be detected. This may be as simple as comparing the actuator position commands to the actuator position and declaring a fault when the error exceeds a threshold over some specified time interval. It would be preferable, however, to not only monitor actuator position but also surface position as well. This would enable one to detect floating surfaces in addition to locked surfaces, both of which can be accommodated by the reconfigurable control system described above. The control law is also flexible enough to handle variations in rate and position limits which might arise from degraded power levels delivered to the actuator or excessive hinge

moments. It would therefore be desirable for the IVHM/FDI to also continually provide estimates of $\overline{\boldsymbol{\delta}}$ and $\underline{\boldsymbol{\delta}}$. The detection of axis saturation by the control allocator that is used attenuate the bandwidth of the explicit models can also be used as an input to the IVHM system to quantify the effect of body-axis rate tracking performance degradation.

E. Results

The results from a nominal run of the simulation will be presented. In this case, all control surfaces are operating normally and the nominal flight path is followed. The first two plots, Figures 3 and 4 show the roll, pitch, and yaw rates. In Figure 3, the commanded and actual rates are displayed and the tracking performance is acceptable. Figure 4 shows the actual and ideal body-axis rates. Here, it is easily seen that the inner-loop response appears to track the response of the ideal first-order lag as the traces in these plots are very similar.

The ideal roll, pitch, and yaw rates correspond to an ideal inner-loop. The ideal inner-loop looks like a first-order system (see Eq. 16). Hence, to test performance of the inner-loop, the commanded roll, pitch, and yaw rates can be filtered by first-order transfer functions and the output of this filter is what is termed the ideal body-axis rates. Comparing the ideal rates with the actual rates provides a measure of the performance of the dynamic inversion and control allocation algorithms. Of course, this is only valid when the commands are feasible.

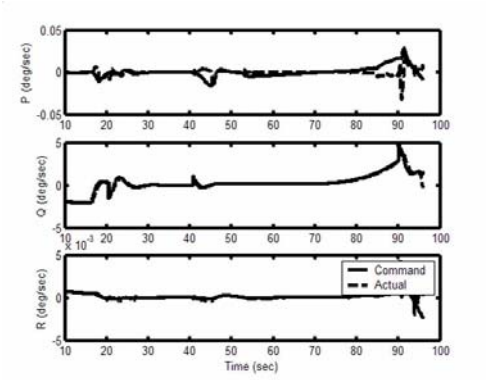

Figure 3. Command and actual body-axis rates - Simulation - nominal.

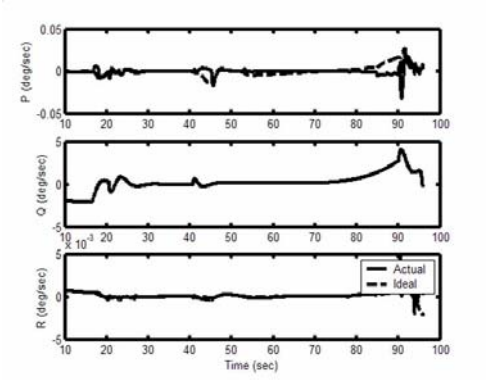

Figure 4. Actual and ideal body-axis rates - Simulation - nominal.

Now, results obtained from simulating a right flaperon failure at 15° will be discussed. This failure results in a large unbalanced rolling moment if no corrective action is taken (and some unbalanced yawing moment). One way to overcome these adverse moments is to move the left flaperon to 15° and use the ruddervators (and bodyflap and speedbrake to a lesser extent) to control the pitching moment. This is exactly how the IAG&C

controller automatically re-mixes the control effectors after the failure. Without an onboard reconfigurable inner-loop, the failed right flaperon causes and uncontrollable rolling moment which is fatal to the vehicle.

Figures 5 and 6 show the body-axis rates for this simulation run. The actual rates track the commands and that the inner-loop control system does behave like a decoupled system of first-order lags. Control

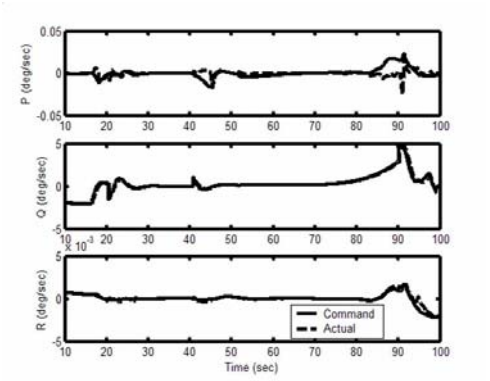

Figure 5. Command and actual body-axis rates - Right Flaperon = 15°, IAG&C controller - Simulation.

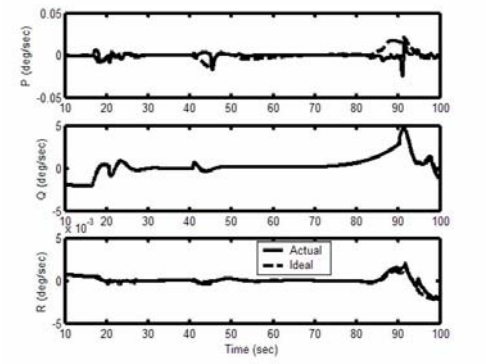

Figure 6. Actual and ideal body-axis rates - Right Flaperon = 15°, IAG&C controller - Simulation.

deflections are shown in Figures 7 and 8. About 41 sec. into the run, a right flaperon failure at 15° occurs. As was stated earlier, this failure causes an adverse rolling moment, which the control allocator overcomes by moving the left flaperon to 15°. Other than a short transient period, the reconfigurable controller is capable of recovering from this type of failure.

III. Effects of Actuator Dynamics on Constrained Control Allocators

Typically, actuator dynamics are ignored when designing flight control allocators for aircraft because the bandwidths of actuators of aerodynamic surfaces are normally much higher than the frequencies of the vehicle's rigid body modes. There are cases however where effector dynamics are not fast enough to warrant this assumption. Typically the response of engine thrust to throttle commands are much slower than aerodynamic surface responses and if aerodynamic surfaces are to be mixed with thrust based control effectors (e.g. X-33 ascent,[8] actuator dynamics may have to be taken into account to achieve an acceptable control design. Even if the nominal actuator dynamics are fast enough to warrant the assumption, changes to the dynamics resulting from degradations to the actuator power source or other malfunction could cause an unacceptable response. Ignoring the interactions between constrained control allocators and actuator dynamics can have serious consequences. Thus, it would be desirable for an IVHM/FDI system to include as an output, estimates of the actuator dynamic model parameters. A method, which post-processes the

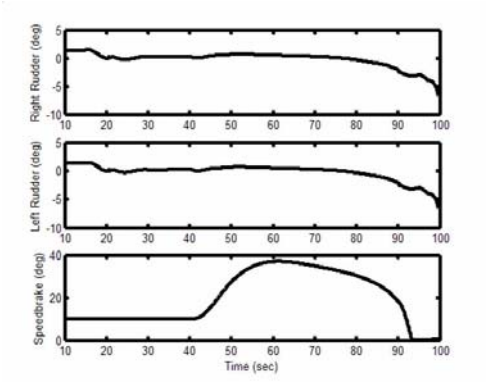

Figure 7. Control Deflections - Right Flaperon = 15°, IAG&C controller - Simulation.

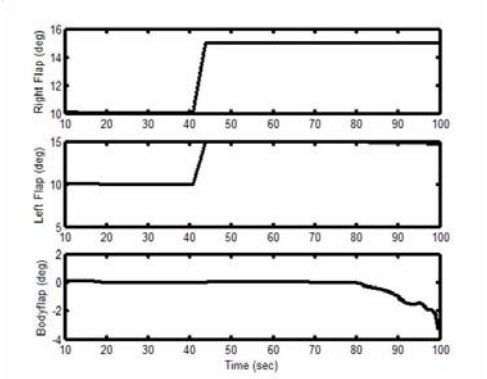

Figure 8. Control Deflections - Right Flaperon = 15°, IAG&C controller - Simulation.

output of a control allocation algorithm, is presented here that can used to compensate for actuator dynamics. While the method was originally intended for un-failed vehicles where the actuator dynamic parameters are know a-priori, there is no reason that it could not be used in conjunction with an IVHM/FDI system that is continually providing instantaneous estimates of these parameters. Results are presented for actuators that have dynamics which are either first-order, second-order with no zeros, or second-order with a single zero. This method solves for a gain, which multiplies the commanded change in control effector setting as computed by the control allocator. This approach is not computationally intensive and thus has the added benefit of being an algorithm which can operate in real-time on a typical flight computer. Likewise, this approach is applicable to both the saturated and unsaturated control effector cases. The basic premise of this method is to post-process the output of the control allocation algorithm to overdrive the actuators so that at the end of a sampling interval, the actual actuator positions are equivalent to the desired actuator positions.

As stated previously, the underlying assumption in most control allocation methods is that actuators respond instantaneously to commands. This assumption may at first seem justified because in practice, actuator dynamics are typically much faster than the rigid body modes that are to be controlled. However, interactions between a constrained control allocator and an actuator with linear dynamics can result in a system that falls well short of its potential. As an example, a simulation was run with a linear programming based control allocation algorithm mixing four control effectors to obtain a desired set of moments, $\mathbf{d}_{des} \in \mathbb{R}^3$. In this simulation, the actuator dynamics for each control effector were set to $\frac{\delta(s)}{\delta_{cmd}(s)} = \frac{5}{s+5}$ and the commanded effector positions, as computed by the control allocator, were used to initialize the allocator at the next timestep. To illustrate the effects of constrained control allocator and actuator dynamics interactions, consider Figures 9 and 10. The objective is to make the accelerations produced by the control effectors ($\mathbf{B}\boldsymbol{\delta}$) equal to the commanded accelerations ($\mathbf{d}_{des}$). Figure 9 shows that when there are no actuator dynamics, the desired result is achieved, namely $\mathbf{B}\boldsymbol{\delta} = \mathbf{d}_{des}$. When actuator dynamics are included, the results are as shown in Figure 10 where it is obvious that $\mathbf{B}\boldsymbol{\delta} \neq \mathbf{d}_{des}$. The scheme presented below, compensates for the effects of actuator dynamics, so that even when actuator dynamics are included, results like those shown in Figure 9 are still obtained. As was shown in the example above, the control allocator/actuator interaction

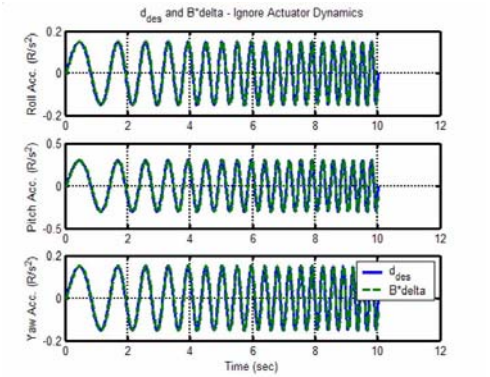

Figure 9. Acceleration Commands and Accelerations Produced by the Controls - No Actuator Dynamics.

can yield control effector positions which produce significantly different accelerations than the commanded accelerations. Bolling[9] has shown that the interaction between first-order actuator dynamics and constrained control allocation algorithms can be eliminated by overdriving the actuators. Here, results for the first-order and second-order actuator dynamics with a zero are provided in detail, along with simulations of both systems.

A. System Definition

Figure 11 shows the system to be analyzed in this work. Inputs to the control allocation algorithm consist of a vector of desired moment or acceleration commands, $\mathbf{d}_{des} \in \mathbb{R}^n$, and a vector containing the current control surface deflections, $\boldsymbol{\delta} \in \mathbb{R}^m$. The output of the control allocator is the commanded control surface deflection vector, $\boldsymbol{\delta}_{cmd} \in \mathbb{R}^m$. The actuator dynamics respond to $\boldsymbol{\delta}_{cmd}$ to produce the actual control deflections,

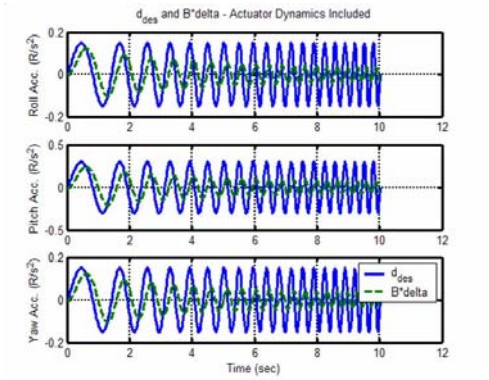

Figure 10. Acceleration Commands and Accelerations Produced by the Controls - Actuator Dynamics Present.

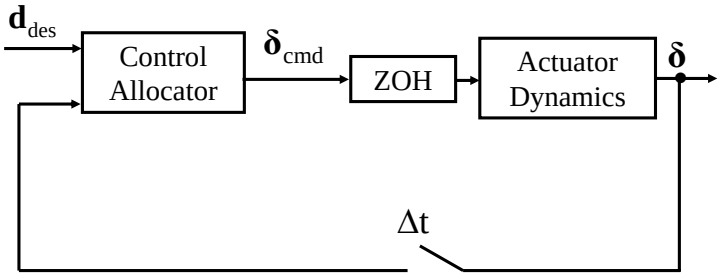

Figure 11. Control allocator and actuator interconnection.

$\boldsymbol{\delta}$. The individual actuators are assumed to have uncoupled dynamics, hardware rate limits $\pm\dot{\boldsymbol{\delta}}_{\max}$, and position limits $\boldsymbol{\delta}_{\min}, \boldsymbol{\delta}_{\max}$. In most control allocator implementations, rate limits are taken into account by converting them into effective position limits at the end of the next sampling period and constraining the effector commands to respect the most restrictive of the rate or position limits, i.e.,

$$\begin{aligned} \overline{\boldsymbol{\delta}} &= \min(\boldsymbol{\delta}_{\max}, \boldsymbol{\delta} + \dot{\boldsymbol{\delta}}_{\max}\Delta t) \\ \underline{\boldsymbol{\delta}} &= \max(\boldsymbol{\delta}_{\min}, \boldsymbol{\delta} - \dot{\boldsymbol{\delta}}_{\max}\Delta t) \end{aligned} \tag{20}$$

where $\boldsymbol{\delta}$ is the current location of the control effectors, $\overline{\boldsymbol{\delta}}, \underline{\boldsymbol{\delta}}$ are the most restrictive upper and lower bounds on the effectors, respectively, and Δt is the sampling period of the digital flight control system.

B. Attenuation of Zero-Order-Hold Inputs For First-Order and Second-Order (No Zeros) Actuator Dynamics

Referring to Figure 11, the desired situation would be for $\boldsymbol{\delta} = \boldsymbol{\delta}_{cmd}$. However, actuator dynamics alter the command signals so that, in general, $\boldsymbol{\delta} \neq \boldsymbol{\delta}_{cmd}$. For actuators with high bandwidths relative to the rigid body modes, this is not a serious concern. However, situations exist where the actuator dynamics are not sufficiently fast and need to be taken into account. In this section, the effects of first-order actuator dynamics on the system shown in Figure 11 will be discussed. Let the dynamics of a single actuator be represented by a continuous time first-order transfer function of the form

$$\frac{\delta(s)}{\delta_{cmd}(s)} = \frac{a}{s+a} \tag{21}$$

The discrete time representation of the first-order actuator dynamics equation is given by

$$\delta(t_{k+1}) = \Phi\delta(t_k) + \Gamma\delta_{cmd}(t_k) \tag{22}$$

where $\Phi \triangleq e^{-a\Delta t}$, $\Gamma \triangleq 1 - e^{-a\Delta t}$, and it has been assumed that the input to the actuator dynamics, $\delta_{cmd}(t_k)$, is held constant over each sampling period. The command to the actuator can be written as

$$\delta_{cmd}(t_k) = \Delta\delta_{cmd_{CA}}(t_k) + \delta(t_k) \tag{23}$$

where the commanded incremental change in actuator position over one timestep is defined by $\Delta\delta_{cmd_{CA}}(t_k) \triangleq \delta_{cmd_{CA}}(t_k) - \delta(t_k)$ and where $\delta_{cmd_{CA}}(t_k)$ is the actuator position command from the control allocator. Since the effector commands are held constant over each sampling period, $\Delta\delta_{cmd_{CA}}(t_k)$ will appear to the actuators to be a step command from the measured position. Recall that $\delta_{cmd_{CA}}(t_k)$ is calculated by the control allocator based upon the assumption that the effector will respond instantaneously to commands. Substituting Equation 23 into Equation 22 yields

$$\delta(t_{k+1}) = \Phi\delta(t_k) + \Gamma\left[\Delta\delta_{cmd_{CA}}(t_k) + \delta(t_k)\right] \tag{24}$$

Since $\Gamma < 1$, the incremental command signal from the control allocation algorithm, $\Delta\delta_{cmd_{CA}}(t_k)$ is attenuated by the actuator dynamics, thus $\delta(t_{k+1}) \neq \delta_{cmd_{CA}}(t_k)$. The objective is to find a gain, M, that modifies the output of the control allocation algorithm such that $\delta(t_{k+1}) = \delta_{cmd_{CA}}(t_k) = \Delta\delta_{cmd_{CA}}(t_k) + \delta(t_k)$. Hence,

$$\delta(t_{k+1}) = \Phi\delta(t_k) + \Gamma\left[M\Delta\delta_{cmd_{CA}}(t_k) + \delta(t_k)\right] \tag{25}$$

and, solving for M yields

$$M = \frac{1}{\Gamma} \tag{26}$$

Thus the actuator command signal must be modified such that

$$\begin{aligned} \tilde{\delta}_{cmd}(t_k) &= M\Delta\delta_{cmd_{CA}}(t_k) + \delta(t_k) \\ &= \frac{1}{\Gamma}\Delta\delta_{cmd_{CA}}(t_k) + \delta(t_k) \end{aligned} \tag{27}$$

Replacing $\delta_{cmd}(t_k)$ in Equation 22 with $\tilde{\delta}_{cmd}(t_k)$ from Equation 27 yields

$$\begin{aligned}\delta(t_{k+1}) &= \Phi\delta(t_k) + \Gamma\tilde{\delta}_{cmd}(t_k) \\ &= \Phi\delta(t_k) + \Gamma\left[\frac{1}{\Gamma}\Delta\delta_{cmd_{CA}}(t_k) + \delta(t_k)\right]\end{aligned} \tag{28}$$

which yields the desired actuator position.

Since Γ can be computed from the known quantities a and Δt, one can compensate for command increment attenuation using Equation 27. For a bank of decoupled first-order actuators with nominal bandwidths of a_i, corresponding values of Γ_i can be computed using $\Gamma_i = (1 - e^{-a_i \Delta t})$. The command increment compensation can then be implemented in discrete time as shown in Figure 12. In Figure 12, the dashed lines are for

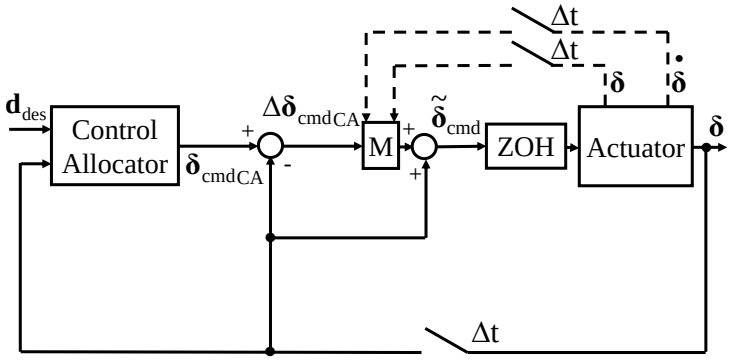

Figure 12. Block diagram of command increment compensation.

compensation for second-order actuator dynamics, as will be discussed shortly, and therefore, are not part of the first-order actuator dynamics compensation scheme. Note that, for multiple actuators, $\mathbf{M}$ in Figure 12 is a diagonal matrix with the entries on the main diagonal being $\Gamma_1, \Gamma_2, \cdots, \Gamma_m$, where the subscript m is defined as the number of control effectors. Hence, the magnitude of the control allocation command increment is modified to counteract the attenuation that results from the interaction between first-order actuator dynamics and the control allocator. Also note that since the method operates in discrete time, it is possible to update $\mathbf{M}$ if an IVHM/FDI system can provide estimates of Φ_i and Γ_i. Such estimates could be potentially be obtained by monitoring actuator commands and measured responses and using least squares based system identification technique (with measures in place to avoid problems with singularities caused by a lack of excitation) to determine an ARMA[10] model of the actuator.

C. Attenuation of Zero-Order-Hold Inputs for Second-Order Actuator Dynamics With A Single Zero

The results of the previous section are now extended to the case of second-order actuator dynamics with a single zero. Let the actuator dynamics be represented by

$$\frac{\delta(s)}{\delta_{cmd}(s)} = \frac{k(s+a)}{s^2 + 2\zeta\omega_n s + \omega_n^2} \tag{29}$$

In this case, it is easily seen that Equation 29 contains derivatives of the input signal. In order to eliminate $\dot{\delta}_{cmd}(t)$, introduce an intermediate variable, $z(s)$, so that

$$\frac{\delta(s)}{z(s)}\frac{z(s)}{\delta_{cmd}(s)} = \frac{k(s+a)}{s^2 + 2\zeta\omega_n s + \omega_n^2} \tag{30}$$

and let

$$\frac{z(s)}{\delta_{cmd}(s)} = \frac{1}{s^2 + 2\zeta\omega_n s + \omega_n^2} \tag{31}$$

and

$$\frac{\delta(s)}{z(s)} = k(s+a) \tag{32}$$

Then, it is easily seen that Equation 31, in state-space form, becomes

$$\begin{bmatrix} \dot{z}(t) \\ \ddot{z}(t) \end{bmatrix} = \begin{bmatrix} 0 & 1 \\ -\omega_n^2 & -2\zeta\omega_n \end{bmatrix} \begin{bmatrix} z(t) \\ \dot{z}(t) \end{bmatrix} + \begin{bmatrix} 0 \\ 1 \end{bmatrix} \delta_{cmd}(t) = \mathbf{A} \begin{bmatrix} z(t) \\ \dot{z}(t) \end{bmatrix} + \mathbf{B}\delta_{cmd}(t) \tag{33}$$

From Equation 32, the output equation becomes

$$\delta(t) = kaz(t) + k\dot{z}(t) = \begin{bmatrix} ka & k \end{bmatrix} \begin{bmatrix} z(t) \\ \dot{z}(t) \end{bmatrix} = \mathbf{C} \begin{bmatrix} z(t) \\ \dot{z}(t) \end{bmatrix} \tag{34}$$

Equations 33 and 34 describe the second-order actuator dynamics.

Using Equations 33 and 34, the discrete-time solution to the second-order actuator dynamics differential equation becomes

$$\begin{gathered} \delta(t_{k+1}) = \left(ka\Phi_{1,1} + k\Phi_{2,1}\right) z(t_k) + \left(ka\Phi_{1,2} + k\Phi_{2,2}\right) \dot{z}(t_k) \\ +\delta_{cmd}(t_k) \int_{t_k}^{t_{k+1}} ka\Phi_{1,2}(t_{k+1} - \tau)d\tau + \delta_{cmd}(t_k) \int_{t_k}^{t_{k+1}} k\Phi_{2,2}(t_{k+1} - \tau)d\tau \end{gathered} \tag{35}$$

where $\mathbf{\Phi}$ is the state transition matrix:

$$\mathbf{\Phi} = e^{\mathbf{A}(t_{k+1} - t_k)} = \begin{bmatrix} \Phi_{1,1} & \Phi_{1,2} \\ \Phi_{2,1} & \Phi_{2,2} \end{bmatrix} \tag{36}$$

Equation 35 can be written as:

$$\delta(t_{k+1}) = D_1 z(t_k) + D_2 \dot{z}(t_k) + \delta_{cmd}(t_k) \left[D_3 + D_4\right] \tag{37}$$

so that

$$\begin{gathered} D_1 = ka\Phi_{1,1} + k\Phi_{2,1} \\ D_2 = ka\Phi_{1,2} + k\Phi_{2,2} \\ D_3 = \int_{t_k}^{t_{k+1}} ka\Phi_{1,2}(t_{k+1} - \tau)d\tau \\ D_4 = \int_{t_k}^{t_{k+1}} k\Phi_{2,2}(t_{k+1} - \tau)d\tau \end{gathered} \tag{38}$$

It is now required to evaluate Φ and perform the math required in Equation 38. By computing the necessary inverse Laplace transforms, it is found that

$$\begin{gathered} \Phi_{1,1} = e^{\sigma\Delta t}\left[\frac{\zeta}{\sqrt{1-\zeta^2}} sin(\omega_d\Delta t) + cos(\omega_d\Delta t)\right] \\ \Phi_{1,2} = \frac{e^{\sigma\Delta t}}{\omega_d} sin(\omega_d\Delta t) \\ \Phi_{2,1} = -{\omega_n}^2 \frac{e^{\sigma\Delta t}}{\omega_d} sin(\omega_d\Delta t) \\ \Phi_{2,2} = e^{\sigma\Delta t}\left[cos(\omega_d\Delta t) - \frac{\zeta}{\sqrt{1-\zeta^2}} sin(\omega_d\Delta t)\right] \end{gathered} \tag{39}$$

where $\omega_d = \omega_n\sqrt{1-\zeta^2}$, $\sigma = -\zeta\omega_n$, and $\Delta t = t_{k+1} - t_k$. Using Equation 38, D_1, D_2, D_3, and D_4 are found to be

$$\begin{gathered} D_1 = kae^{\sigma\Delta t}\left[\frac{\zeta}{\sqrt{1-\zeta^2}} sin(\omega_d\Delta t) + cos(\omega_d\Delta t)\right] - k{\omega_n}^2 \frac{e^{\sigma\Delta t}}{\omega_d} sin(\omega_d\Delta t) \\ D_2 = \frac{kae^{\sigma\Delta t}}{\omega_d} sin(\omega_d\Delta t) + ke^{\sigma\Delta t}\left[cos(\omega_d\Delta t) - \frac{\zeta}{\sqrt{1-\zeta^2}} sin(\omega_d\Delta t)\right] \\ D_3 = \frac{ka}{\omega_d\omega_n^2}\left[\omega_d + e^{\sigma\Delta t}\left\{\sigma sin(\omega_d\Delta t) - \omega_d cos(\omega_d\Delta t)\right\}\right] \\ D_4 = \frac{k}{\omega_n^2}\left[-\sigma + e^{\sigma\Delta t}\left\{\sigma cos(\omega_d\Delta t) + \omega_d sin(\omega_d\Delta t)\right\}\right] + \frac{k\zeta}{\omega_d\omega_n}\left[-\omega_d - e^{\sigma\Delta t}\left\{\sigma sin(\omega_d\Delta t) - \omega_d cos(\omega_d\Delta t)\right\}\right] \end{gathered} \tag{40}$$

The objective is to find a gain M that will modify $\Delta\delta_{cmd_{CA}}(t_k)$ in such a way that $\delta(t_{k+1}) = \delta_{cmd_{CA}}(t_k)$. Hence, it is desired to find M such that

$$\Delta\delta_{cmd_{CA}}(t_k) + \delta(t_k) = D_1 z(t_k) + D_2 \dot{z}(t_k) + (D_3 + D_4)\left[M\Delta\delta_{cmd_{CA}}(t_k) + \delta(t_k)\right] \tag{41}$$

Solving for M gives

$$M = \frac{\Delta\delta_{cmd_{CA}}(t_k) + (1 - D_3 - D_4)\delta(t_k) - D_1 z(t_k) - D_2 \dot{z}(t_k)}{(D_3 + D_4)\Delta\delta_{cmd_{CA}}(t_k)} \tag{42}$$

In this case, it can be seen that not only is the actual actuator position needed, so are the intermediate variables $z(t_k)$ and $\dot{z}(t_k)$. In practice, an estimator (for example, a Kalman filter) would be designed to provide $z(t_k)$ and $\dot{z}(t_k)$. As with the first-order case, for a system with more than one actuator, $\mathbf{M}$ in Figure 12 would be a diagonal matrix with entries along the main diagonal being $M_1, M_2, \cdots, M_m$. Here, M_i would be computed using Equation 42 and ω_{n_i}, ζ_i corresponding to the i^{th} actuator.

D. Simulation Results

In this section, results from a simulation of the system displayed in Figure 12 will be shown. A rate and position constrained linear programming based control allocator will be utilized in this work. In this case, the control allocation algorithm's objective, referring to Figure 11, is to find $\boldsymbol{\delta}_{cmd}$ such that

$$\mathbf{d}_{des} = \mathbf{B}\boldsymbol{\delta}_{cmd} \tag{43}$$

where $\mathbf{B}$ is the control effectiveness matrix and $\mathbf{d}_{des}$ is typically a set of moment or acceleration commands for the roll, pitch, and yaw axes. Although, if feasible, the control allocator will be able to find a $\boldsymbol{\delta}_{cmd}$ such that Equation 43 holds, the real test is to determine what happens after the actuator dynamics operate on $\boldsymbol{\delta}_{cmd}$. Hence, the overall system goal is to achieve $\boldsymbol{\delta}$ such that

$$\mathbf{d}_{des} = \mathbf{B}\boldsymbol{\delta} \tag{44}$$

Equation 44 is the metric upon which the quality of results will be judged. In this example, four control effectors are present and the control effectiveness matrix is fixed at

$$\mathbf{B} = \begin{bmatrix} -0.4 & 0.4 & -0.1 & 0.1 \\ -0.1 & -0.1 & -0.6 & -0.6 \\ -0.1 & 0.1 & -0.1 & 0.1 \end{bmatrix} \tag{45}$$

where the elements of $\mathbf{B}$ have units of $(rad/sec^2)/deg$. Since there are more control effectors (4) than axes to control (3), a control mixed or allocator must be used. In this work, a flight-tested linear programming based control allocation algorithm with rate and position limiting will be used.[3,11] It is important to note, however, that any control allocation method could be used.

In the following simulations, a mixture of actuator dynamics will be used. Specifically, the dynamics of each actuator are

$$\begin{array}{c} \frac{\delta_1(s)}{\delta_{cmd_1}(s)} = \frac{2.5(s+10)}{s^2+7.071s+25} \\ \frac{\delta_2(s)}{\delta_{cmd_2}(s)} = \frac{2.5(s+10)}{s^2+7.071s+25} \\ \frac{\delta_3(s)}{\delta_{cmd_3}(s)} = \frac{49}{s^2+7s+49} \\ \frac{\delta_4(s)}{\delta_{cmd_4}(s)} = \frac{5}{s+5} \end{array} \tag{46}$$

which gives $\zeta = \frac{\sqrt{2}}{2}$, $\omega_n = 5$, $k = 2.5$ for the second-order with zero cases, $\zeta = 0.5$, $\omega_n = 7$, $k = 49$ for the simple second-order case, and $a = 10$. Each actuator is rate and position limited by the following values

$$\begin{aligned} \boldsymbol{\delta}_{min} &= \begin{bmatrix} -1.5 & -1.5 & -1.5 & -1.5 \end{bmatrix} (\text{deg}) \\ \boldsymbol{\delta}_{max} &= \begin{bmatrix} 0.4 & 1.5 & 1.5 & 1.5 \end{bmatrix} (\text{deg}) \\ \dot{\boldsymbol{\delta}}_{max_{CA}} &= \begin{bmatrix} 10 & 10 & 10 & 3 \end{bmatrix} \left(\frac{\text{deg}}{\text{sec}}\right) \end{aligned} \tag{47}$$

These limits were selected so that at least one position and one rate limit were in effect at some time during the simulation. This was done to show that the method developed in this work is applicable when control effectors are saturated. As will be shown, when compensation is used, actuator 1 becomes upper position limited and actuator 4 becomes rate limited as the frequency of the commands increases. The command signals, $\mathbf{d}_{des}$, consist of chirps of magnitude $0.15, 0.3,$ and $0.15\ \frac{rad}{sec^2}$ in the roll, pitch, and yaw channels and where the frequency ranged from $0.5 - 2$ Hz as a linear function of time over a 10 sec time interval.

Simulation runs were performed with and without compensation for magnitude attenuation due to actuator dynamics. Ideal conditions are when the actuator dynamics can be represented by $\frac{\delta(s)}{\delta_{cmd}(s)} = 1$. If sufficient control authority and ideal conditions exist, then the control system would achieve $\mathbf{d}_{des} = \mathbf{B}\boldsymbol{\delta}$, which is the best possible performance. Figures 13 and 14 show $\mathbf{d}_{des}$ and $\mathbf{B}\boldsymbol{\delta}$ without and with the magnitude compensation described in Equations 26 and 42 applied. Clearly, when the magnitude compensation is not used (Figure 13), $\mathbf{d}_{des} \neq \mathbf{B}\boldsymbol{\delta}$, and a large error exists between these two quantities. When magnitude compensation is used (Figure 14), however, $\mathbf{d}_{des} \cong \mathbf{B}\boldsymbol{\delta}$ and near ideal performance is achieved. Figures 15 and 16 display the control effector commands, $\boldsymbol{\delta}_{cmd_{CA}}$, and actual deflections, $\boldsymbol{\delta}$, when magnitude compensation is used. In this case, the actual deflections are nearly equal to the commands and as a result, $\mathbf{d}_{des} \cong \mathbf{B}\boldsymbol{\delta}$. Notice that control effector 1 is upper position limited and control effector 4 is rate limited for the last few seconds of the simulation run. Thus, using the simple gain adjustment described in this work results in the actual control deflections being equal to the commanded control deflections. It is apparent that adjusting the control effector command increments can help to mitigate adverse interactions between discrete time implementations of control allocation algorithms and actuator dynamics.

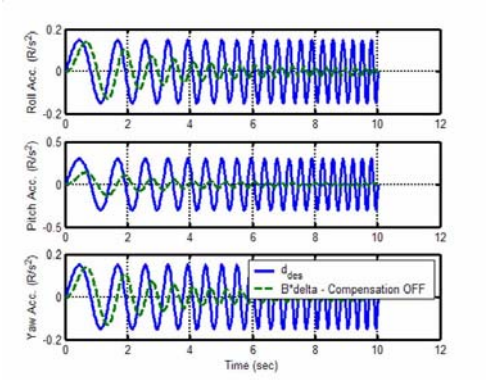

Figure 13. Commanded ($\mathbf{d}_{des}$) and simulated ($\mathbf{B}\boldsymbol{\delta}$) angular accelerations $\left(\frac{rad}{sec^2}\right)$ - Compensation OFF.

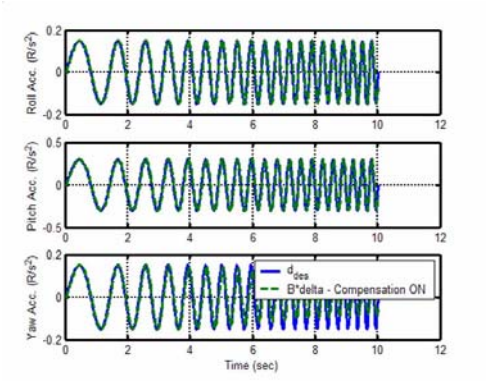

Figure 14. Commanded ($\mathbf{d}_{des}$) and simulated ($\mathbf{B}\boldsymbol{\delta}$) angular accelerations $\left(\frac{rad}{sec^2}\right)$ - Compensation ON.

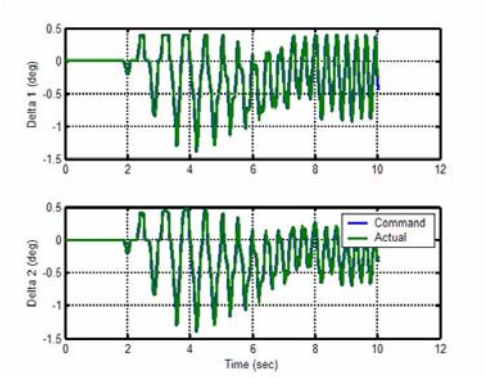

Figure 15. Control Effector 1 and 2 Positions - Compensation ON.

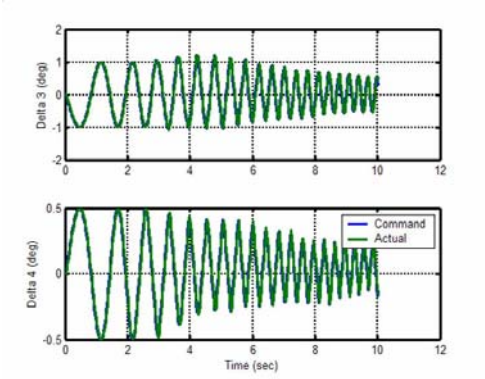

Figure 16. Control Effector 3 and 4 Positions - Compensation ON.

IV. Identification of Control Effectiveness

In the event of control effector damage or failures, one of several static approaches to on-line system identification can be used[8, 12–15] to estimate current values of a vehicle's control derivatives. The newly updated control derivatives can then used by the dynamic inversion control law to provide enhanced tracking performance in the prescence of failures, damage or modeling error. These static identification approaches provide direct, non-iterative solutions for control derivatives and provide safeguards against singularities caused by insufficient excitation. This protection makes use of a-priori knowledge of the effectiveness of the control surfaces in order to for a set of stochastic constraints. In cases where insufficient signal content exists to make a reliable measurement based estimate, the solutions approach the a-priori estimates. Control derivative estimates can sometimes be improved by lengthening the time over which data is collected which increases the likelihood that some excitation will occur; however, it will result in a trade-off with the speed of response of the identification algorithm. Other measures, such as control effector dithering or null-space signal injection[8, 13] can be employed to reduce the probability of being forced to revert to a-priori control derivative estimates .

The static identification method described below illustrates how one can estimate the control derivatives for a vehicle with n control effectors. Without loss of generality, the following discussion will focus on the estimation of the roll control derivatives $\dot{p}_{\delta_1}$, ..., $\dot{p}_{\delta_n}$ associated with the control effectors δ_1, ..., δ_n. To illustrate the process we analyze the roll-axis. The calculation of pitch and yaw axis control derivatives is analogous to the procedure describe to estimate the roll derivatives

The roll acceleration equation of motion in the stability axis is given by:

$$\begin{aligned} \dot{p} = \dot{p}_\beta \beta + \dot{p}_r r + \dot{p}_p p + \dot{p}_{pq} pq + \dot{p}_{\delta_1} \delta_1 + \cdots \\ + \dot{p}_{\delta_{12}} \delta_{12} + w_p + \text{ higher order terms} \end{aligned} \tag{48}$$

The rolling acceleration coefficients due to side-slip β, yaw rate r, roll rate p, and pitch rate q are $\dot{p}_\beta$, $\dot{p}_r$, $\dot{p}_p$, and $\dot{p}_q$ respectively. The roll acceleration coefficients due to the n control effectors δ_1, ..., δ_n are $\dot{p}_{\delta_1}$, ..., $\dot{p}_{\delta_n}$ respectively. Sensor measurement noise is represented by w_p and we note that in practice angular accelerations must be estimated using high-pass filtered rate gyro measurements as direct measurements of angular acceleration are not generally available from inertial measurement units.

To estimate the new control derivatives, we first remove contributions of the side-slip, pitch rate, roll rate, yaw rate, and the higher order terms from (48):

$$\begin{aligned} \dot{\tilde{p}} = \dot{p} - [\dot{p}_\beta \beta + \dot{p}_r r + \dot{p}_p p + \dot{p}_{pq} pq + \\ \text{higher order terms}] = \dot{p}_{\delta_1} \delta_1 + \cdots + \dot{p}_{\delta_n} \delta_n \end{aligned} \tag{49}$$

Concatenating k sampled measurements in Equation (49), we have a data window of length k resulting in:

$$\underbrace{\begin{bmatrix} \dot{\tilde{p}}_1 \\ \vdots \\ \dot{\tilde{p}}_k \end{bmatrix}}_{Z} = \underbrace{\begin{bmatrix} \delta_{1_1} & \delta_{2_1} & \cdots & \delta_{n_1} \\ \vdots & \vdots & \vdots & \vdots \\ \delta_{1_k} & \delta_{2_k} & \cdots & \delta_{n_k} \end{bmatrix}}_{H} \underbrace{\begin{bmatrix} \dot{p}_{\delta_1} \\ \vdots \\ \dot{p}_{\delta_n} \end{bmatrix}}_{\Theta} + \underbrace{\begin{bmatrix} w_{p_1} \\ \vdots \\ w_{p_k} \end{bmatrix}}_{W} \tag{50}$$

or more compactly,

$$Z = H\Theta + W$$

where Z denotes a $k \times 1$ vector of measured roll accelerations due to the control effectors. H is a $k \times n$ regressor matrix of measured control surface deflections. The $n \times 1$ vector Θ is the rolling moment coefficients to be estimated. The W represents the system sensor noise. The $n \times 1$ vector W is described by stochastic process of zero mean with the covariance $R(\theta) = r(\theta) I_k$. The minimum-variance estimate[12] $\hat{\Theta}_{mv}$ of Θ is then

$$\hat{\Theta}_{mv} = (H^T R^{-1} H)^{-1} H^T R^{-1} Z$$

The standard of deviation of the estimate $\hat{\Theta}$ is then:

$$\hat{\sigma} = \sqrt{(\tilde{Z}^T \tilde{Z})/(k-n)}$$

where $\tilde{Z} = Z - H\hat{\Theta}$ is the return difference. The corresponding covariance P_{mv} of the estimate $\hat{\Theta}_{mv}$ is

$$P_{mv} = \hat{\sigma}^2 (H^T H)^{-1}$$

A priori information about the parameters to be estimated, such as the control derivative of the nominal aircraft can be used at this point to provide a mixed estimate of the minimum-variance estimate and a priori values. The a priori values $\Theta_{apriori}$ with its associated covariance Q becomes the stochastic constraint on the final mixed estimate $\hat{\Theta}_{me}$ and its covariance:

$$\begin{aligned} \hat{\Theta}_{me} &= \hat{\Theta}_{mv} + P_{mv}(P_{mv} + Q)^{-1}(\Theta_{apriori} - \hat{\Theta}_{mv}) \\ P_{me} &= [I - P_{mv}(P_{mv} + Q)]P_{mv} \end{aligned}$$

In calculating the mixed estimate $\hat{\Theta}_{me}$, the $k \times n$ moving data window H is updated by replacing the earliest values of the control surface deflections with their latest values. The same is done for the $k \times 1$ vector Z of the roll accelerations. Finally, the mixed estimate results $\hat{\Theta}_{me}$ are often low-pass filtered to smooth out the final results.

The identification of control derivatives is desirable for cases where the effectors are damaged or only partially effective. If control effectors are locked, floating or if actuator performance is degraded, it would be more desirable to obtain critical reconfigurable control information directly from an IVHM/FDI as this avoids many of the complications associated with control derivative estimation.

In the example below taken from,[?] a dynamic inversion based adaptive reconfigurable controller was augmented with with the above identification method to estimate control derivatives for the X-33 's twelve control effectors when the right flap δ_1 fails by floating at 20 seconds. The vehicle has twelve control effectors to generate the pitching, rolling and yawing moments. These control effectors consist of eight aerodynamic control surfaces: left and right body flaps δ_1, δ_2; left and right rudders δ_3,δ_4; left and right inboard elevons δ_5, δ_6 as well as left and right outboard elevons δ_7, δ_8. The vehicle's propulsion-based control effectors include the left and right top engine quadrants δ_9, δ_{10} and the left and right bottom engine quadrants δ_{11}, δ_{12} repectively. Due to their large size and locations, the body flaps are the most effective of the eight aero-control surfaces. The engine quadrants; however are the most effective of all twelve control effectors. The uncertainties associated with the control effectivess parameters are directly reflected in their covariances. The uncertainties can depend on the flight conditions and the quality of experimental data. The covariance of the effectors' a priori rolling accelerations are chosen to be $r(\delta_1) = r(\delta_2) = 0.01$, and $r(\delta_3) = \cdots = r(\delta_8) = 0.001$ and $r(\delta_9) = \cdots = r(\delta_{12}) = 0.0001$. Because of their large effectiveness relative to the other aero-control surfaces and the air flow interaction on their large surface, the covariance of the a priori estimates of the body-flap control effectiveness parameters are chosen to be larger than those of the the less effective aero-control surfaces. The covariances associated with the engine quadrants are chosen to be smaller than those of the aero-control surfaces because the propulsive forces generated by the engine are less uncertain.

With the loss of the right flap and *without* the on-line system identification the controller fails to adapt to the changing rolling moment effectiveness, thus it is unable to track the guidance commands as seen in Figure 17. Under failure and *with* on-line system identification one can see that the controller is able to track the guidance commands. The value of the mixed estimate of the right flap rolling control derivative is shown in Figure 18. It is observed that rapid variation of the right flap's control derivative estimate is caused by the change in the slope of the roll command. The sensitivity of the right flap's estimate to the roll command can be reduced by choosing a slower filter (the baseline filter is first order with a 15 rad/sec break frequency). Furthermore, at lower dynamic pressure the aero control effectors $\delta_1 \cdots \delta_8$ are less effective. This occurs for time > 150 seconds. The rolling accelerations produced by the aero-effectors are thus small in equation (49) while the engine differential throttle effectors $\delta_9 \cdots \delta_{12}$ are large. This difference in the effectiveness among the vehicle's effectors cause wide fluctuations in the estimates of the aero-effectors' control derivative.

In Figure 17, the right flap failure occurs 20 seconds into flight and the vehicle begins to depart at approximately 110 seconds. The ability of the vehicle to remain stable for 70 seconds following the loss of the right body flap without system identification can be attributed in part to the dominance of the propulsion based effectors in the early portion of the flight.

Figure 18,shows the the rolling moment control derivative estimates $L_{\delta_{flap}}$ for the left and right body flaps. They are fully dimensionalized and not normalized by the dynamic pressure $\bar{q}$. The a priori values of the roll derivatives are the outputs of a polynominal fit of the experimental data which depend on the vehicle's angle of attack, sideslip angle, altitude, and velocity. The roll control derivative of the left body

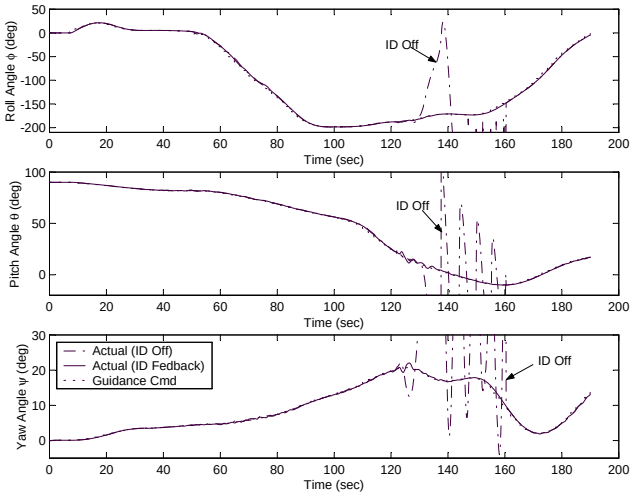

Figure 17. Attitude tracking performance with lost right flap.

flap is underestimated compared to its a priori values. The roll control derivative of the missing right body flap fluctuates about zero as expected. Exact matching of the roll control derivatives to the a priori value for the left body flap and zero for the missing right body flap may be difficult to obtain since these parameters vary within the data window. These estimation errors are compensated by the robustness of the dynamic inversion control law.

Null Space Injection

As mentioned earlier system identification techniques require input and output excitation in order to obtain reliable measurement based estimates. In order to identify elements of the control effectiveness matrix, each control effector must be active at all times. Furthermore, each effector must be moving independently so that there is no correlation between the movement of one control effector and another. Decorrelated control deflections are necessary to obtain a well conditioned regressor matrix H for system identification. The addition of small zero-mean signals to the actuator commands, sometimes called dithering, can be used to provide an acceptable level of input excitation. Unfortunately this simple approach results in degraded vehicle response since in general $\mathbf{B}(\boldsymbol{\delta}+\boldsymbol{\delta}_{\mathbf{dither}}) \neq \mathbf{d}_{\mathbf{des}}$. One solution to this problem is to provide a dithering signal that lies in the null space of the $\mathbf{B}$, i.e. $\mathbf{B}\boldsymbol{\delta}_{\mathbf{dither}} = \mathbf{0}$ so that $\mathbf{B}(\boldsymbol{\delta} + \boldsymbol{\delta}_{\mathbf{dither}}) = \mathbf{d}_{\mathbf{des}}$. This can be accomplished indirectly by randomly perturbing the control effector preference vector according to:

$$\boldsymbol{\delta}_{\mathbf{p}} \triangleq \mathbf{W}^{-\mathbf{1}}\mathbf{B}^{\mathbf{T}}(\mathbf{B}\mathbf{W}^{-\mathbf{1}}\mathbf{B}^{\mathbf{T}})^{-\mathbf{1}}\mathbf{d}_{\mathbf{des}} \tag{51}$$

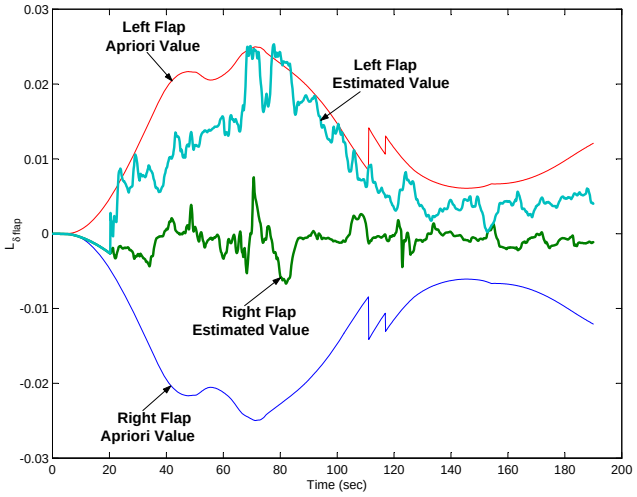

Figure 18. Estimates of left and (failed) right flaps roll control derivatives (ID on at 20 sec)

where

$$\begin{aligned} \mathbf{W} &= \tilde{\mathbf{W}}\mathbf{W_r} \\ \mathbf{W_r} &= \mathrm{diag}(\mathbf{10^{v_1}}, \mathbf{10^{v_2}} \cdots \mathbf{10^{v_m}}) \end{aligned} \tag{52}$$

and $\mathbf{v}$ is a vector of uniformly distributed random variables between -1 and 1. The matrix $\tilde{\mathbf{W}}$ is a nominal diagonal weighting matrix used for scaling purposes to equally distribute commands. Note that $\boldsymbol{\delta}_p$ is actually the solution to a weighted least squares problem:

$$\begin{aligned} \min_{\boldsymbol{\delta}} J &= \boldsymbol{\delta}^T \mathbf{W} \boldsymbol{\delta} \\ \text{subject to:} & \\ \mathbf{B}\boldsymbol{\delta} &= \mathbf{d_{des}} \end{aligned} \tag{53}$$

Thus the preference vector will be driven toward a randomly weighted least squares solution to the control allocation problem that does not account for rate and position constraints. Now the preference vector $\boldsymbol{\delta}_p$ is randomly changing and the sufficiency branch of the LP-based control allocation ensures that $\mathbf{B}\boldsymbol{\delta} = \mathbf{d_{des}}$ and that the control effector constraints are not violated. This approach ensures that the control effectors are decorrelated and active without degrading the vehicle response. This approach also avoids the explicit calculation of the null space of $\mathbf{B}$.

Figure 19 shows the response of the control effectors and the tracking performance of the X-33 operating in the null-space-injection mode. One can see that the control effectors appear to be quite active and

decorrelated while the tracking performance is well behaved. Figure 20 shows the effector response and tracking performance of the X-33 operating with minimum-deflection control allocation. The differences between the null-space injection mode and the minimum deflection mode can easily be seen. In the minimum deflection mode, one can see that several of the effectors are completely inactive while others are correlated. The vehicle tracking performance is good as well.

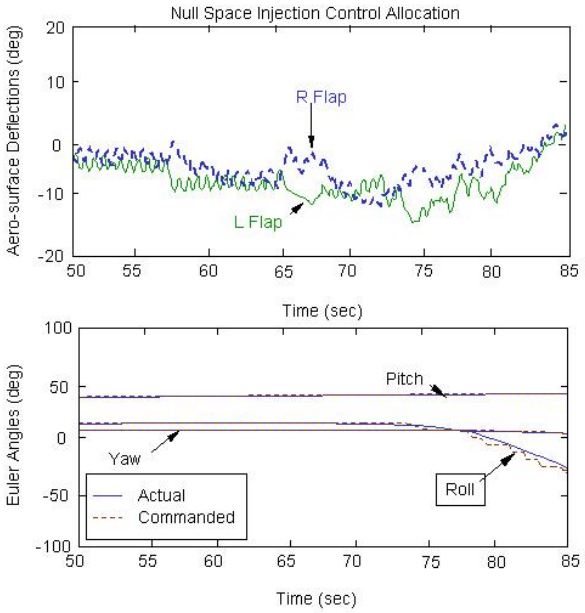

-0

Figure 19. Attitude tracking using dynamic inversion/null-space injection control allocation

A. Interaction with IVHM/FDI

The opportunity for IVHM/FDI to make use of the information obtained from on-line system identification exists. It may be possible to use control derivative estimates as described above as part of a damage or health assessment. This may be particulary useful for vehicles that lack a comprehensive sensor suite capable of directly sensing damage. The rapid identification of vehicle damage is important for trajectory reshaping as well since such algorithms implicitly rely on accurate predictions of vehicle aerodynamics at flight conditions beyond the point at which damage is detected.

V. Constraint Estimation and Damage Recovery

The trend towards the development of autonomous vehicles has placed more emphasis on requiring trajectory retargeting/reshaping algorithms. One of the main difficulties in trajectory reshaping is predicting the effects of failures or damage at future flight conditions. Here a method is presented that can generate critical information that is required to perform on-line trajectory reshaping. In particular, a method for estimating failure induced constraints, for failures involving locked or floating control effectors, is presented which accounts for 6 degree-of-freedom (DOF) effects upon the reduced order models that are used by trajectory generation algorithms. As will be demonstrated, these constraints on the vehicle are not constant and can vary widely as flight conditions change. This means that one cannot assume that a set of constraints estimated at a one flight condition will be valid at any other flight condition. Effector failures such as locked or floating surfaces are a class of failures whose effects can be estimated over a wide range of operating conditions. This is because the aerodynamic database for the vehicle does not change as a result of such a failure. The effects of locked or floating surfaces can be estimated at all flight conditions for which the original aerodynamic database is valid.

In order to facilitate practical on-line trajectory reshaping , vehicle constraints and aerodynamic proper-

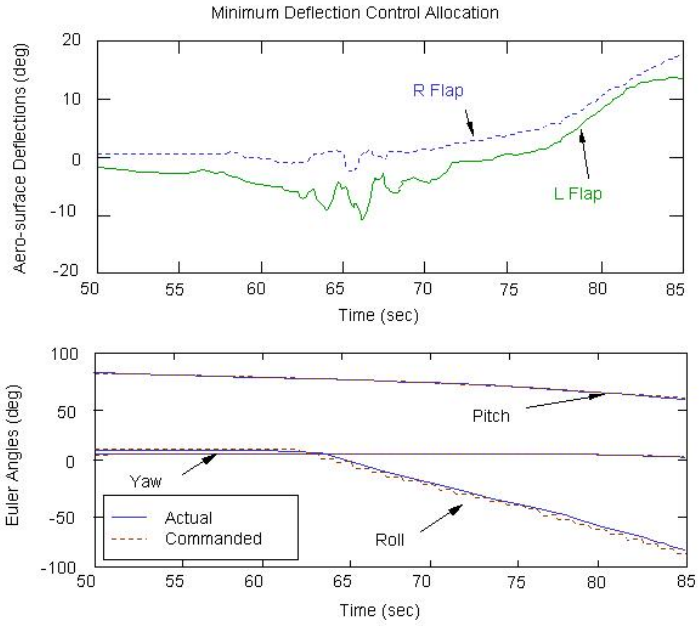

-0

Figure 20. Attitude tracking using dynamic inversion/minimum deflection control allocation

ties must be estimated at flight conditions beyond the point at which the failure is detected. This requirement contrasts sharply with that of inner-loop reconfigurable control where one only requires a snapshot of the current model parameters that can either be obtained through on-line system identification or directly from IVHM/FDI. While the problem of estimating the effects of locked or floating effector failures over the flight envelope is tractable due to invariance of the aerodynamic database, techniques for estimating the effects of damage over the flight envelope are nascent. There have been some recent efforts to develop algorithms for predicting the effects of damage over the flight envelope that will require an extensive amount of information from an IVHM system.[16,17] These prediction methods will require outer-mold-line information, presumably obtained from an advanced IVHM system, to drive fast aerodynamic prediction codes such as DATCOM[18] that can generate estimates of aerodynamic coefficients that can be blended with temporally local estimates from system identification algorithms. The degree of difficulty in obtaining accurate estimates depends upon the flight condition at which the damage occurs. For example, if damage occurs in the hypersonic flight regime, one does not expect to see large changes in the aerodynamic coefficients until the aircraft approaches the transsonic flight regime where the aerodynamic characteristics are often highly sensitive to changes in Mach number.

The computation of reshaped trajectories online requires that two major issues be solved:

1. Flight certifiable algorithms must be developed so that trajectories can be computed on-line.

2. The effects of failures or damage on the vehicle model and vehicle constraints must be quantified.

To illustrate the varying nature of reduced order aerodynamic models and constraints, a vehicle, for which an aerodynamic database is available, was selected for this analysis. It is assumed that the sideslip angle $\beta = 0$ and that symmetric flight conditions exist. Therefore, the lateral directional wing-body forces and moments will be assumed to be zero. Thus, only longitudinal motion will be considered.

To begin the analysis, the wing-body pitching moment coefficient of the vehicle is calculated at each data point (j, i) in a grid spanning the regions of interest in the aerodynamic database, giving

$$C_{m_{oj,i}} = f\left(M_j, \alpha_i\right) \tag{54}$$

where $C_{m_{oj,i}} = C_{m_{oj,i}}(M_j, \alpha_i)$ is the base pitching moment coefficient at the j^{th} Mach (M_j) and i^{th} angle of attack (α_i) data point. Since only longitudinal motion is considered here, it is assumed that $C_{rm_{oj,i}}(M_j, \alpha_i) = 0$ and $C_{ym_{oj,i}}(M_j, \alpha_i) = 0$, where $C_{rm_{oj,i}}(M_j, \alpha_i)$, $C_{ym_{oj,i}}(M_j, \alpha_i)$ are the base rolling and

yawing moment coefficients at the (j,i) data point, respectively. Now that the wing-body pitching moment has been computed, a control allocation scheme is used to provide the control effector settings, $\boldsymbol{\delta}_{j,i} \in \mathbb{R}^m$ (m = number of control effectors), that rotationally trim the vehicle. Hence, at each point in the Mach-α envelope, it is desired to find $\boldsymbol{\delta}_{j,i}$ such that

$$\begin{pmatrix} C_{rm_{\delta_{j,i}}}(M_j,\alpha_i,\boldsymbol{\delta}_{j,i}) \\ C_{m_{\delta_{j,i}}}(M_j,\alpha_i,\boldsymbol{\delta}_{j,i}) \\ C_{ym_{\delta_{j,i}}}(M_j,\alpha_i,\boldsymbol{\delta}_{j,i}) \end{pmatrix} = \begin{pmatrix} 0 \\ -C_{m_{oj,i}}(M_j,\alpha_i) \\ 0 \end{pmatrix} \tag{55}$$

where $C_{rm_{\delta_{j,i}}}(M_j,\alpha_i,\boldsymbol{\delta}_{j,i})$, $C_{m_{\delta_{j,i}}}(M_j,\alpha_i,\boldsymbol{\delta}_{j,i})$, and $C_{ym_{\delta_{j,i}}}(M_j,\alpha_i,\boldsymbol{\delta}_{j,i})$ are the rolling, pitching, and yawing moment coefficients produced by the control effectors.

All control effectors are position limited so that $\underline{\boldsymbol{\delta}} \leq \boldsymbol{\delta}_{j,i} \leq \overline{\boldsymbol{\delta}}$ where $\underline{\boldsymbol{\delta}}$ and $\overline{\boldsymbol{\delta}}$ are vectors whose elements correspond to the lower and upper limits of the k^{th} control surface. Without loss of generality, locked control effectors are characterized by $\underline{\boldsymbol{\delta}}_k = \overline{\boldsymbol{\delta}}_k$, while floating control effectors are characterized by their lack of moment generating capability, i.e., $C_{rm_{\delta_{j,i}}} = C_{m_{\delta_{j,i}}} = C_{ym_{\delta_{j,i}}} = 0$. We utilize a piecewise linear constrained control allocator[19] to find the appropriate value of $\boldsymbol{\delta}_{j,i}$ which satisfies Equation 55. Let $\boldsymbol{\delta}^*_{j,i}$ denote a solution to Equation 55. If $\boldsymbol{\delta}^*_{j,i}$ can be found such that Equation 55 is satisfied, then sufficient control power exists to longitudinally trim the vehicle. On the other hand, if Equation 55 is not satisfied, then a deficiency exists. By performing this test at each Mach-α point, a rotational trim deficiency map can be constructed. This map indicates where the vehicle is longitudinally trimmable; hence, the map displays trim information for all Mach numbers and angles of attack in the aerodynamic database. In particular, when a point in the deficiency map is zero, then that point is declared longitudinally trimmable; when there is a nonzero value, then a deficiency exists and that point is not trimmable. Thus, from this information, one can determine the range of trimmable angle of attack.

Similar to generating the trim deficiency map, trim force coefficient maps can be created. These maps provide the lift and drag at every operating condition for which a model is available. The lift and drag can be computed at each operating point by substituting the solution to Equation 55, $\boldsymbol{\delta}^*_{j,i}$, into the aerodynamic database and calculating the trim lift and drag coefficients. The total lift and drag coefficients are given by the sum of the wing-body and control surface coefficients for a given Mach-α pair and corresponding $\boldsymbol{\delta}^*_{j,i}$:

$$\begin{aligned} C_L(M_j,\alpha_i) &= C_{L_o}(M_j,\alpha_i) + C_{L_{\delta^*_{j,i}}}\left(M_j,\alpha_i,\boldsymbol{\delta}^*_{j,i}\right) \\ C_D(M_j,\alpha_i) &= C_{D_o}(M_j,\alpha_i) + C_{D_{\delta^*_{j,i}}}\left(M_j,\alpha_i,\boldsymbol{\delta}^*_{j,i}\right) \end{aligned} \tag{56}$$

where $C_L(M_j,\alpha_i)$ and $C_D(M_j,\alpha_i)$ are the total lift and drag coefficients, $C_{L_o}(M_j,\alpha_i)$ represents the wing-body lift coefficient, $C_{D_o}(M_j,\alpha_i)$ represents the sum of the wing-body induced and parasitic drag coefficients, and $C_{L_{\delta^*_{j,i}}}\left(M_j,\alpha_i,\boldsymbol{\delta}^*_{j,i}\right), C_{D_{\delta^*_{j,i}}}\left(M_j,\alpha_i,\boldsymbol{\delta}^*_{j,i}\right)$ are the sum of the lift and drag coefficients produced by the control effectors, respectively.

The algorithm to compute pitch deficiency, lift, and drag maps and to determine the range of trimmable angle of attack is summarized as follows:

1. Define a grid for Mach and Angle of Attack, including lower and upper bounds and step size
2. Initialize $\boldsymbol{\delta}$
3. Loop 1 $\rightarrow$ For j = 1 to Number of Machs
4. Loop 2 $\rightarrow$ For i = 1 to Number of Angle of Attacks
5. Compute the wing-body pitching moment coefficient, $C_{m_{oj,i}}(M_j,\alpha_i)$
6. Solve a control allocation problem to find $\boldsymbol{\delta}^*_{j,i}$ which satisfies Equation 55
7. Compute trim deficiency at each point, i.e., deficiency(j,i) = $\left\| \begin{bmatrix} 0 \\ -C_{m_{oj,i}}(M_j,\alpha_i) \\ 0 \end{bmatrix} - \begin{bmatrix} C_{rm_{\delta_{j,i}}}(M_j,\alpha_i,\boldsymbol{\delta}_{j,i}) \\ C_{m_{\delta_{j,i}}}(M_j,\alpha_i,\boldsymbol{\delta}_{j,i}) \\ C_{ym_{\delta_{j,i}}}(M_j,\alpha_i,\boldsymbol{\delta}_{j,i}) \end{bmatrix} \right\|_2$

8. If deficiency(j,i) = 0, then the corresponding Mach-α combination is trimmable
9. Compute drag and lift at each data point by substituting $\boldsymbol{\delta}^*_{j,i}$ into the aerodynamic database
10. Increment Mach and/or Alpha
11. End Angle of Attack loop
12. End Mach loop

This algorithm yields the control deficiency map as well as the lift and drag maps. Each map is valid for all operating conditions for which a model is available.

A. Constraint Estimation Example

As examples, we consider 2 different vehicles. The first is a reentry vehicle with 8 control effectors. The technique described in Section V is used to compare the trim maps and trim force coefficients of the nominal vehicle to those of a failed vehicle. Figure 21 displays the rotational trim deficiency map for the un-failed

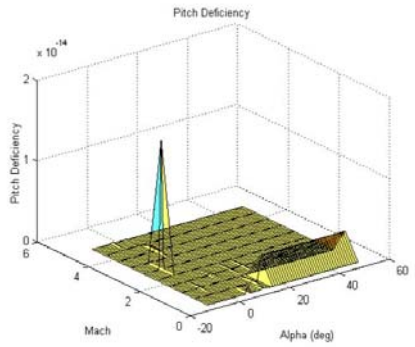

Figure 21. Pitch Deficiency For Nominal Vehicle.

vehicle. It is easily discernable that there are no combinations of Mach-α for which the vehicle is not statically longitudinally trimmable, as all of the deficiency values are quite small. As expected from the deficiency map in Figure 21, the range of trimmable angle of attack is $-10°$ to $50°$ for all Mach numbers, since there are no locations which display rotational trim deficiency. Figure 22 displays the pitch deficiency map for a failure of

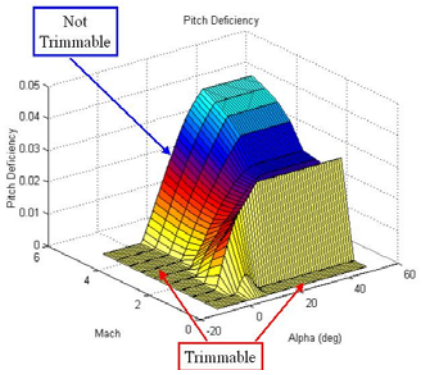

Figure 22. Pitch Deficiency For Failed Left and Right Body Flaps at 26°.

both bodyflaps at $26°$. Figure 22 immediately portrays the feasible range of angle of attack (angle of attack values for which the trim deficiency map is zero). For a trajectory which would span the entire Mach range

shown here, it can be seen that the range of feasible angle of attack is much smaller than the range of the nominal case. In fact, the feasible region of angle of attack and Mach number reduces to a corridor on the Mach-α grid, as illustrated in Figure 23. This corridor corresponds to angle of attack values which are less than about 3°. Once the trim deficiency map has been created, a simple interpolation scheme can be used

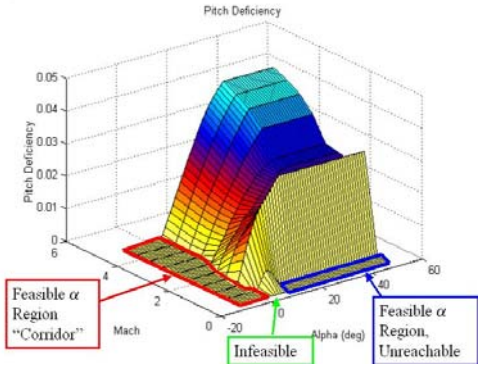

Figure 23. Pitch Deficiency: Feasible α Corridor And Unreachable Regions.

to define the boundary between the trimmable and non-trimmable regions. In this way, one can determine the range of trimmable angle of attack for all Mach numbers of interest. Now, the trim force coefficients will be investigated. Figures 26 and 27 illustrate the effect of a failure upon the drag and lift forces for a re-entry vehicle where the sizes of the control surfaces are relatively large. This vehicle has at its disposal 6 control effectors: left/right flaperons, left/right ruddervators, a speedbrake, and a bodyflap. Here, it is easily discernable that the failure of both ruddervators at 5° has caused a large change in drag and lift as compared to the nominal case. For this vehicle, the ruddervators are extremely powerful and hence, large changes in drag and lift are observed.

One of the key points to all of this is that the failure induced constraints, be it trimmable angle of attack, drag, or lift are not constant from one flight condition to another. For example, consider Figure 22. Assume that at Mach 5 during a flight, both bodyflaps fail at 26°. If an algorithm were to compute the range of trimmable angle of attack at that instant, the range would be from $-10°$ to about 3°. Typically, this information would be used by a trajectory retargeting algorithm to compute a new trajectory to finish the mission. However, this information is not sufficient for a trajectory retargeting algorithm because the range of trimmable angle of attack is not constant. As seen in Figure 22, from Mach 2.5 to Mach 0.5, the range of trimmable angle of attack shrinks to about $-10°$ to $-2°$. Hence, the effects of failures, at future flight conditions can change and must be computed for use in a retargeting algorithm. The procedure developed in this work allows calculation of the effects of failures at every flight condition defined in the aerodynamic model. Coupling the range of trimmable angle of attack with drag and lift maps for a full-envelope of operating conditions provides a trajectory retargeting algorithm the information required to compute a feasible trajectory, if possible, throughout the remaining flight regime, given the vehicle's limitations.

VI. Summary of Requirements for IVHM/FDI Systems from a Guidance, Control and Trajectory Reshaping Perspective

Throughout this manuscript, numerous requirements and opportunities for synergistic information exchange between IVHM/FDI systems and guidance, control and trajectory reshaping algorithms have been identified. Many of these requirements will require advances in IVHM/FDI capabilities in order to realize a high level of fault and damage tolerance. A list of desirable capabilities is provided below:

- Continuous estimates of control effector health

  Actuator rate and position limits

  Power and hinge moment limits

  Dynamic model parameters

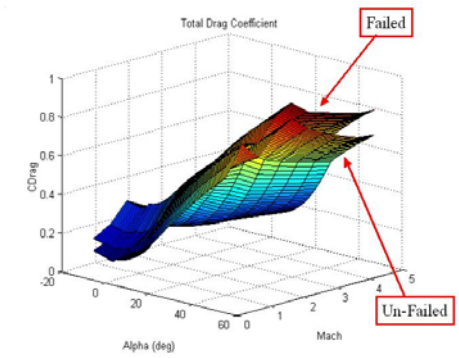

Figure 24. Drag Coefficient For Failed And Un-Failed Configurations.

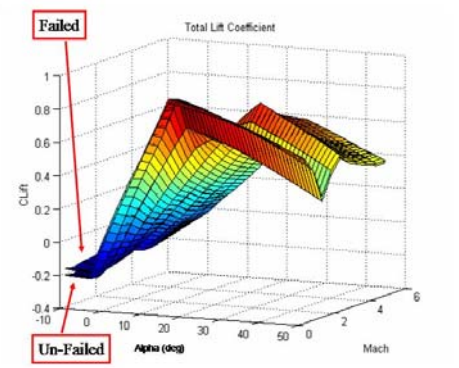

Figure 25. Lift Coefficient For Failed And Un-Failed Configurations.

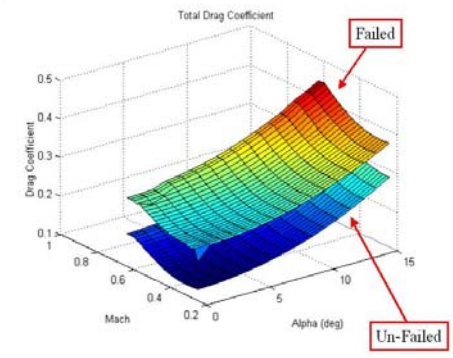

Figure 26. Drag Coefficient For A Vehicle Whose Control Surfaces Are Large Relative To The Wing-Body.

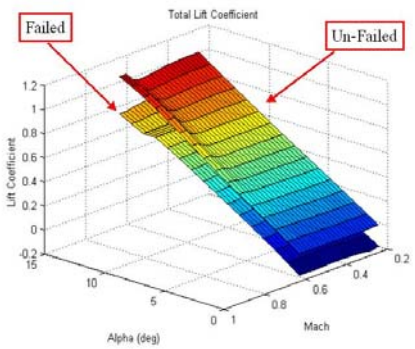

Figure 27. Lift Coefficient For A Vehicle Whose Control Surfaces Are Large Relative To The Wing-Body.

Separately monitor actuator and effector rates and positions

Incorporate system identification results into health assessments

- Estimation of vehicle mass properties

  Mass property variation due to fuel burn

  Mass property variation due to damage

- Estimate outer mold line of wing-body
- Constraint Estimation for Trajectory

  Dynamic pressure

  Load factor

  Angle of attack

  Thermal

- Engine failures (quantify performance loss)

VII. Conclusions

The integration of health management, fault detection and isolation with trajectory reshaping and adaptive guidance and control is a natural and necessary step in producing reliable and responsive autonomous aerospace vehicles. The benefits of reconfigurable control and trajectory reshaping have been demonstrated; however, in many cases these results relied upon the assumption that IVHM/FDI systems provided specific information to the algorithms. Requirements on IVHM/FDI from the perspective of guidance, control and trajectory reshaping have been listed community have listed and some opportunities for beneficial information exchange between the two systems have been identified.

References

[1] "Application of Multivariable Control Theory to Aircraft Control Laws," Tech. Rep. WL-TR-96-3099, Wright Laboratory, WPAFB, OH, 1996.

[2] A. B. Page and M. L. Steinberg, "A Closed-loop Comparison of Control Allocation Methods," in *Proceedings of the 2000 Guidance, Navigation and Control Conference*, AIAA 2000-4538, August 2000.

[3] M. Bodson, "Evaluation of optimization methods for control allocation," *Journal of Guidance, Control and Dynamics*, vol. 25, no. 4, pp. 703–711, 2002.

[4] J. R. H. J. D. Schierman and D. G. Ward, "Adaptive Guidance With Trajectory Reshaping For Reusable Launch Vehicles," in *Proceedings of the 2002 Guidance, Navigation and Control Conference*, AIAA 2002-4458, August 2002.

[5]

[6] B. Etkin, *Dynamics of Atmospheric Flight*. John Wiley & Sons, Inc., 1972.

[7]D. B. Doman and A. G. Sparks, "Concepts for constrained control allocation of mixed quadratic and linear effectors," in *Proceedings of the 2002 American Control Conference*, ACC02-AIAA1028, May 2002.

[8]

[9]J. G. Bolling, "Implementation of constrained control allocation techniques using an aerodynamic model of an f-15 aircraft," Master's thesis, Virginia Polytechnic Institute and State University, 1997.

[10]J. D. P. Gene F. Franklin and M. L. Workman, *Digital Control of Dynamic Systems*. New York, NY: Addison-Wesley, 1989, pp. 366-395.

[11]D. B. Doman and M. W. Oppenheimer, " Improving Control Allocation Accuracy for Nonlinear Aircraft Dynamics," in *Proceedings of the 2002 Guidance, Navigation and Control Conference*, AIAA Paper No. 2002-4667, August 2002.

[12]P. R. Chandler, M. Pachter, and M. Mears, "System identification for adaptive and reconfigurable control," *Journal of Guidance, Control and Dynamics*, vol. 18, pp. 516–524, May-June 1995.

[13]J. M. Buffington, P. Chandler, and M. Pachter, " Integration of On-line System Identification and Optimization-based Control Allocation," Tech. Rep. AIAA Paper 98-4487, American Institute of Aeronautics and Astronautics, 1998.

[14]D. Ward and R. Barron, "A self-designing receding horizon optimal flight controller," in *Proceedings of the American Control Conference*, IEEE, June 1995.

[15]J. F. M. David G. Ward and M. Bodson, "Development and flight testing of a parameter identification algorithm for reconfigurable control," *Journal of Guidance, Control, and Dynamics*, vol. 21, no. 6, pp. 948–956, 1998.

[16]A. Verma, M. Oppenheimer, and D. Doman, "Online adaptive estimation and trajectory reshaping," in *Proceedings of the 2005 Guidance, Navigation and Control Conference*, AIAA Paper No. 2005-6436, August 2005.

[17]D. Allwine, J. Fisher, J. Strahler, D. Lawrence, M. Oppenheimer, and D. Doman, "Online trajectory generation for hypersonic vehicles," in *Proceedings of the 2005 Guidance, Navigation and Control Conference*, AIAA Paper No. 2005-6435, August 2005.

[18]W. B. Blake, "Missile Datcom User's Manual - 1997 FORTRAN 90 Revision," Tech. Rep. VA-WP-TR-1998-3009, AFRL, WPAFB, OH, Aug. 1998.

[19]M. Bolender and D. B. Doman, "Non-linear control allocation using piecewise linear functions," in *Proceedings of the 2003 Guidance, Navigation and Control Conference*, AIAA 2003-5357, August 2003.